

## Supplementary Materials for

### A nuclease that mediates cell death induced by DNA damage and poly(ADP-ribose) polymerase-1

Yingfei Wang,\* Ran An, George K. Umanah, Hyejin Park, Kalyani Nambiar, Stephen M. Eacker, BongWoo Kim, Lei Bao, Maged M. Harraz, Calvin Chang, Rong Chen, Jennifer E. Wang, Tae-In Kam, Jun Seop Jeong, Zhi Xie, Stewart Neifert, Jiang Qian, Shaida A. Andrabi, Seth Blackshaw, Heng Zhu, Hongjun Song, Guo-li Ming, Valina L. Dawson,\*  
Ted M. Dawson\*

\*Corresponding author. Email: [tdawson@jhmi.edu](mailto:tdawson@jhmi.edu) (T.M.D.); [vdawson1@jhmi.edu](mailto:vdawson1@jhmi.edu) (V.L.D.);  
[yingfei.wang@utsouthwestern.edu](mailto:yingfei.wang@utsouthwestern.edu) (Y.W.)

Published 7 October 2016, *Science* **353**, aad6782 (2016)  
DOI: 10.1126/science.aad6872

#### This PDF file includes

Supplementary Text  
Figs. S1 to S17  
Tables S1 and S2  
References

## Supplementary Text

### Analysis of MIF Protein Structure

The core PD-D/E(X)K topology structure of nucleases consists of 4 $\beta$ -strands next to two-helices (19). Two of the  $\beta$ -strands are parallel to each other whereas the other two are antiparallel (fig. S3C, modified from (19)). Previous 3-D crystal structures of MIF indicate that it exists as a trimer (22-24). The trimeric structure of MIF enables the interaction of the  $\beta$ -strands of each monomer with the other monomers resulting in a PD-D/E(X)K structure that consists of 4  $\beta$ -strands next to 2  $\alpha$ -strands (Fig. 1E and fig. S3, D to G). Two of the  $\beta$ -strands ( $\beta$ -4 and  $\beta$ -5) are parallel whereas the other two strands ( $\beta$ -6 and  $\beta$ -7) (from the adjacent monomer) are anti-parallel (fig. S3, D to G). The topology structure of PD-D/E(X)K motifs with orientations of the beta-strands relative to the alpha helices in the MIF trimer are very similar to EcoRV, a well characterized endonuclease (fig. S3, H to K). Importantly, the PD-D/E(X)K motif based on the trimer structure of MIF is structurally similar to type II ATP independent restriction endonucleases, such as EcoRI and EcoRV, as well as, ExoIII family purinic/apyrimidinic (AP) endonucleases, such as ExoIII (Fig. 1E and fig. S3, L to N). Moreover, MIF also has a similar topology to the PvuII endonuclease and its  $\beta$ -7 strand is of similar size to PvuII endonuclease  $\beta$ -strand at the same position in its PD-D/E(x)K motif (fig. S3O). These 3-D modeling results taken together indicate that MIF belongs to the PD-D/E(X)K nuclease-like superfamily (25, 26).

### Identification of Key Residues Critical for MIF's Nuclease Activity

To identify amino acid residues critical for MIF's nuclease activity, key aspartates and glutamates residues within the PD-D/E(X)K domains of MIF were mutated to alanine. Substitution of glutamate 22 by alanine (E22A) clearly but not completely reduces MIF's nuclease activity, whereas alanine substitutions at the other aspartates and glutamates including D17A, D45A, E55A, E86A, D93A and D101A have no substantial effect (fig. S4E). Mutation of the CxxCxxHx<sub>(n)</sub>C zinc finger domain of MIF to C57A;C60A has no appreciable effect (fig. S4E). Since MIF E22A has reduced nuclease activity, additional conserved mutations around E22 were made (fig. S4, F and G). We find that MIF E22Q has no nuclease activity (Fig. 2D and fig. S4,D and H), whereas E22D has equivalent nuclease activity to wild-type (Fig. 2D). These data suggest that this glutamic acid residue (E22) in the first  $\alpha$ -helix of MIF is critical for its nuclease activity, which is consistent with prior reports that this glutamic acid in the first  $\alpha$ -helix of many Exonuclease-Endonuclease-Phosphatase (EEP) domain superfamily nucleases is highly conserved and it is the active site for nuclease activity (25, 26). Based on 3-dimensional structural modeling (Fig. 1E), possible MIF DNA binding sites were mutated including: P16A, P44A, R87Q, R89Q, P92A, D45Q, D17Q, E55Q, and D93Q (fig. S4H). We find that P16A or D17Q prevents MIF nuclease activity (fig. S4H). Based on both the sequence alignment and 3-dimensional structural modeling of MIF, our data reveal that P16, D17 and E22 are within the same PD-D/E(X)K motif and mutation of each single residue is sufficient to block MIF nuclease activity. Considering the fact that E22 in the first  $\alpha$ -helix is highly conserved across species and previously it has been reported as an

active site for PD-D/E(X)K nuclease-like superfamily nuclease activity (25, 26), we focused on the E22 mutant in subsequent studies.

#### EndoG and Cyclophilin A are not Directly Involved in PARP-1 Dependent Large DNA Fragmentation

EndoG and cyclophilin A have been previously suggested to be AIF associated nucleases (12, 50, 51). Pulsed-field gel electrophoresis indicates that EndoG cleaves DNA into small fragments that are not consistent with the larger DNA fragmentation pattern observed in parthanatos (fig. S4D). In contrast, MIF cleaves DNA into large fragments with a pattern similar to MNNG induced DNA fragments (Fig. 2B and fig. S4D) (13, 15). Cyclophilin A and AIF have no obvious nuclease activity with glutathione S-transferase (GST) serving as a negative control (fig. S4D).

#### MIF Nuclease Activity is Independent of its Oxidoreductase and Tautomerase Activities

Previous studies indicate that MIF has both oxidoreductase and tautomerase activities (28, 30, 31). The oxidoreductase activity of wild-type and MIF mutants were measured using insulin as a substrate in which reduced insulin exhibits an optical density value of 650 nm in the presence of wild-type MIF (fig. S5A). E22Q, E22A, C57A;C60A MIF mutants and the tautomerase P2G MIF mutant have no appreciable effects on MIF's oxidoreductase activity (fig. S5A). MIF's tautomerase activity was also measured. E22Q, E22A, C57A;C60A MIF mutations have no appreciable effect on MIF's tautomerase activity whereas the P2G MIF mutant significantly reduces MIF's tautomerase activity (fig. S5B). These results taken together indicate that MIF active site mutants E22Q and E22A have no appreciable effect on MIF's oxidoreductase or tautomerase activities.

#### Purified MIF Proteins have no Adventitious Nuclease Contamination

To confirm that the recombinant MIF preparations did not contain an adventitious nuclease, FPLC was performed. FPLC reveals only one peak at a molecular weight of approximately 37 kD consistent with MIF existing as a trimer. MIF E22Q and E22A also elute at 37 kD consistent with a trimer structure suggesting that these mutations do not appreciably affect the confirmation of MIF (fig. S5C). Coomassie blue staining reveals only a single band in the proteins following FPLC purification (fig. S5D) as well as proteins without FPLC purification (fig. S4G). Both types of proteins with and without FPLC purification were used in the nuclease assays and no obvious difference was observed. The purity of all these recombinant MIF proteins used in the nuclease assays was also confirmed by two-independent mass spectrometry (MS) assays. The majority of peptides identified by MS are MIF. No known nuclease from all species that can cleave single or double stranded DNA was identified. Thus, MIF preparations are highly pure and no adventitious nuclease is present.

#### MIF Protein Confirmation is Unaffected by E22Q, E22A and C57A;C60A Mutations

Far-ultraviolet (UV) circular dichroism (CD) spectroscopy, a common method to study protein secondary structure shows that wild-type MIF is composed of a mixture of  $\alpha$ -helices and  $\beta$ -sheets in agreement with the previously reported crystal structure of MIF (23). MIF mutants, E22Q, E22A and C57A;C60A, show similar CD spectra as wild-type

MIF suggesting that these mutations do not significantly affect the conformation of MIF (fig. S5E). No significant change is observed on the addition of Mg<sup>2+</sup> to wild-type MIF or MIF mutants (fig. S5F-I). However, addition of Zn<sup>2+</sup> promotes large changes in the spectra indicating significant changes in the structure of the wild-type MIF protein on Zn<sup>2+</sup> binding (fig. S5F). MIF E22Q and E22A show a similar CD spectra as wild-type MIF in the presence of Zn<sup>2+</sup> (fig. S5, G and H), however the addition of Zn<sup>2+</sup> to the C57A;C60A mutant did not cause a change in the CD spectra indicating that MIF binds Zn<sup>2+</sup> at the CxxCxxHx<sub>(n)</sub>C zinc finger domain of MIF (fig. S5I).

Near UV CD spectroscopy was used to further analyze the tertiary structure of MIF and MIF mutants. The purified proteins have a properly folded tertiary structure since there are distinct peaks of phenylalanine and tyrosine in the near UV CD spectra (fig. S5J). MIF mutants, E22Q, E22A and C57A;C60A, show similar near UV CD spectra as wild-type suggesting that these mutations do not significantly affect the tertiary structure of MIF (fig. S5, J to M). The addition of Mg<sup>2+</sup> to wild-type MIF or the MIF mutant C57A;C60A causes a significant change in tertiary structure indicative of Mg<sup>2+</sup> binding (fig. S5, J and M). The E22A shows minor changes in the presence of Mg<sup>2+</sup> and the E22Q shows no significant changes in the near UV CD spectra suggesting that Mg<sup>2+</sup> binds at or near E22 (fig. S5, K and L), which is consistent with our finding that Mg<sup>2+</sup> is required for MIF's nuclease activity and E22Q and E22A mutants can block its nuclease activity completely or partially. The addition of Zn<sup>2+</sup> to wild-type MIF or MIF mutants E22A and E22Q causes a significant change in the tertiary structure indicative of Zn<sup>2+</sup> binding whereas the MIF C57A;C60A mutant exhibits no significant change consistent with the Zn<sup>2+</sup> binding to the CxxCxxHx<sub>(n)</sub>C zinc finger domain (fig. S5, J to M).

#### ChIP Sequencing Analysis of MIF-DNA Binding Properties

Since our data shows that MIF has nuclease activity, next we further studied whether MIF binds to DNA in HeLa cells treated with DMSO or MNNG (50 μM, 15 min). 5 hours after the treatment, cells were cross-linked and prepared for ChIP assays followed by deep sequencing. The quality of sheared genomic DNA and the specificity of ChIP using the MIF antibody was tested and confirmed (fig. S6, A and B). After excluding overlapped peaks in the DMSO-treated samples, 0.1% of total mapped reads exhibit MIF peaks after MNNG treatment (fig. S6C). MIF preferentially binds to the promoter and 5' UTR regions after MNNG treatment (fig. S6D). The representative IGV visualization of MIF enrichment on the genome is shown in two different window sizes (250 kb (fig. S6E) and 50 kb (fig. S6F). The average distance intervals between MIF peaks are about 15 to 60 kb, which is consistent with size of DNA fragments observed via pulse-gel electrophoresis during parthanatos. ChIP-qPCR further confirms that MIF binds to the peak regions at 55101, 66005, 65892, 36229, 46426 and 62750 but it does not bind to the non-peak regions after MNNG treatment (fig. S6G).

#### Mapping AIF-MIF Interactions

To confirm that MIF is an AIF interacting protein, GST pull down experiments were performed. Wild-type GST-AIF pulls down endogenous MIF and wild-type GST-MIF pulls down endogenous AIF (Fig. 4A and fig. S10, A to D). The domain that binds MIF was further defined by GST pull downs with various GST-tagged AIF domains (fig. S10A). MIF binds to GST-C2b AIF (aa 551-590) and GST C2e AIF (aa 571-612) (fig.

S10, A and B). MIF does not bind to GST-C2aAIF, GST-C2cAIF, GST-C2dAIF or GST indicating that it does not nonspecifically bind to GST at the experimental conditions used (fig. S10, A and B). Mutating aa567-592 into polyalanines (AIFm567-592) or deleting aa567-592 (AIF $\Delta$ 567-592) from full length completely abolished MIF and AIF binding (fig. S10C), suggesting that MIF binds to AIF at aa 567-592.

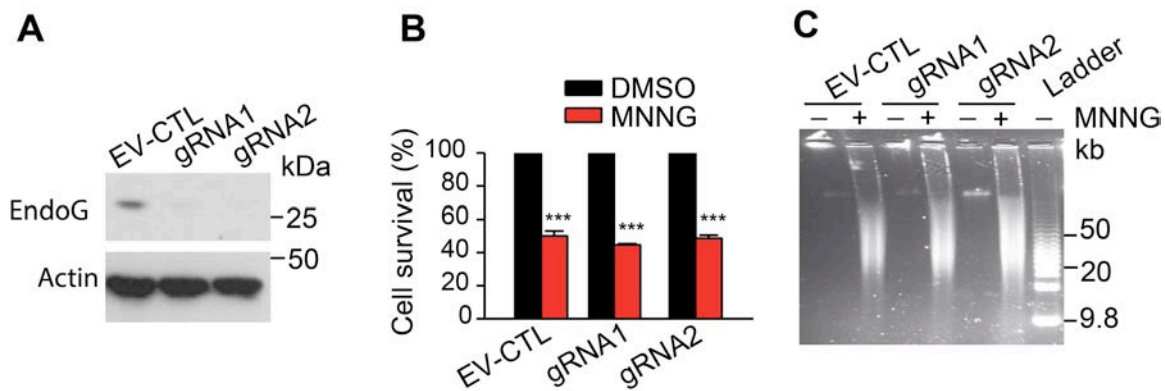


**Fig. S1.**

**EndoG is not required for PARP-1 dependent cell death.** (A) Knockout of EndoG using CRISPR-Cas9 system in SH-SY5Y cells. EV-CTL, empty vector control. (B) Effects of EndoG knockout on MNNG-induced cell death. (C) Effects of EndoG knockout on MNNG caused DNA damage.

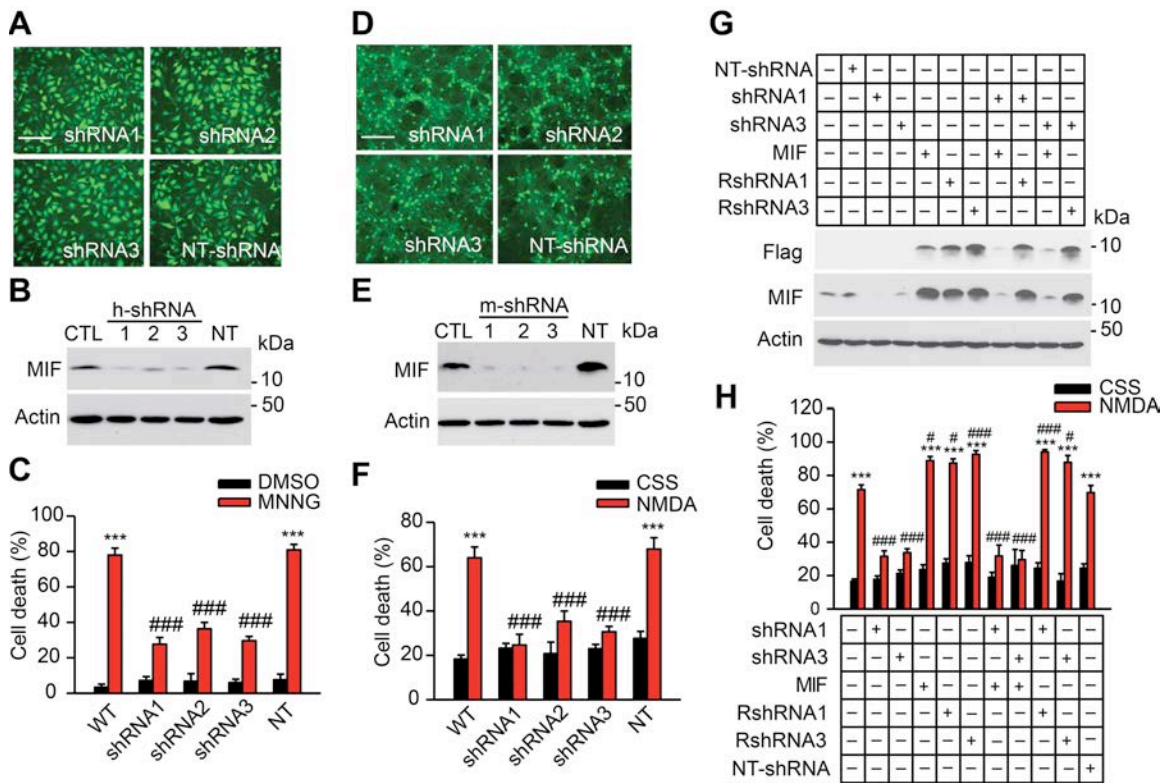


**Fig. S2**

**MIF knock down protects cells from MNNG and NMDA-induced cell death.**

(A) Representative images of HeLa cells transduced with human MIF shRNA1-3 IRES-GFP lentivirus or non-targeting (NT) shRNA IRES-GFP lentivirus. (B) MIF protein levels in HeLa cells after shRNA transduction. hMIF shRNA 1, 2 and 3 caused  $83.3 \pm 7.1\%$ ,  $71.6 \pm 3.2\%$ , and  $82.7 \pm 6.3\%$  MIF protein reduction, respectively in HeLa cells. CTL, control. (C) Quantification of MNNG ( $50 \mu\text{M}$ , 15 min)-induced HeLa cell death. Means  $\pm$  SEM are shown. \*\*\* $P < 0.001$ , versus DMSO control. # $P < 0.001$ , versus WT with MNNG treatment. (D) Representative images of cortical neurons transduced with mouse MIF shRNA1-3 IRES-GFP or NT-shRNA IRES-GFP lentivirus. (E) MIF protein levels in cortical neurons after shRNA transduction. (F) Quantification of NMDA ( $500 \mu\text{M}$ , 5 min)-induced neuronal cell death in MIF knockdown neurons. mMIF shRNA 1, 2 and 3 caused  $84.5 \pm 8.2\%$ ,  $90.1 \pm 7.1\%$ , and  $92.2 \pm 3.3\%$  MIF protein reduction, respectively in cortical neurons. CSS, controlled salt solution. Means  $\pm$  SEM are shown. \*\*\* $P < 0.001$ , versus CSS control. # $P < 0.001$ , versus WT with NMDA treatment. (G) Representative immunoblots of MIF knockdown and overexpression of MIF mutants, which are resistant to shRNA1 and 3 in cortical neurons. (H) Quantification of NMDA-induced neuronal cell death in MIF knockdown cortical neurons and cells overexpressing MIF mutants, which are resistant to shRNA1 and 3. Means  $\pm$  SEM are shown. \*\*\* $P < 0.001$ , versus CSS control. # $P < 0.001$ , versus WT with NMDA treatment, one-way ANOVA. Scale bar,  $100 \mu\text{m}$ . Intensity of MIF signal is shown in C, F & H. The experiments were repeated in 3 independent trials.

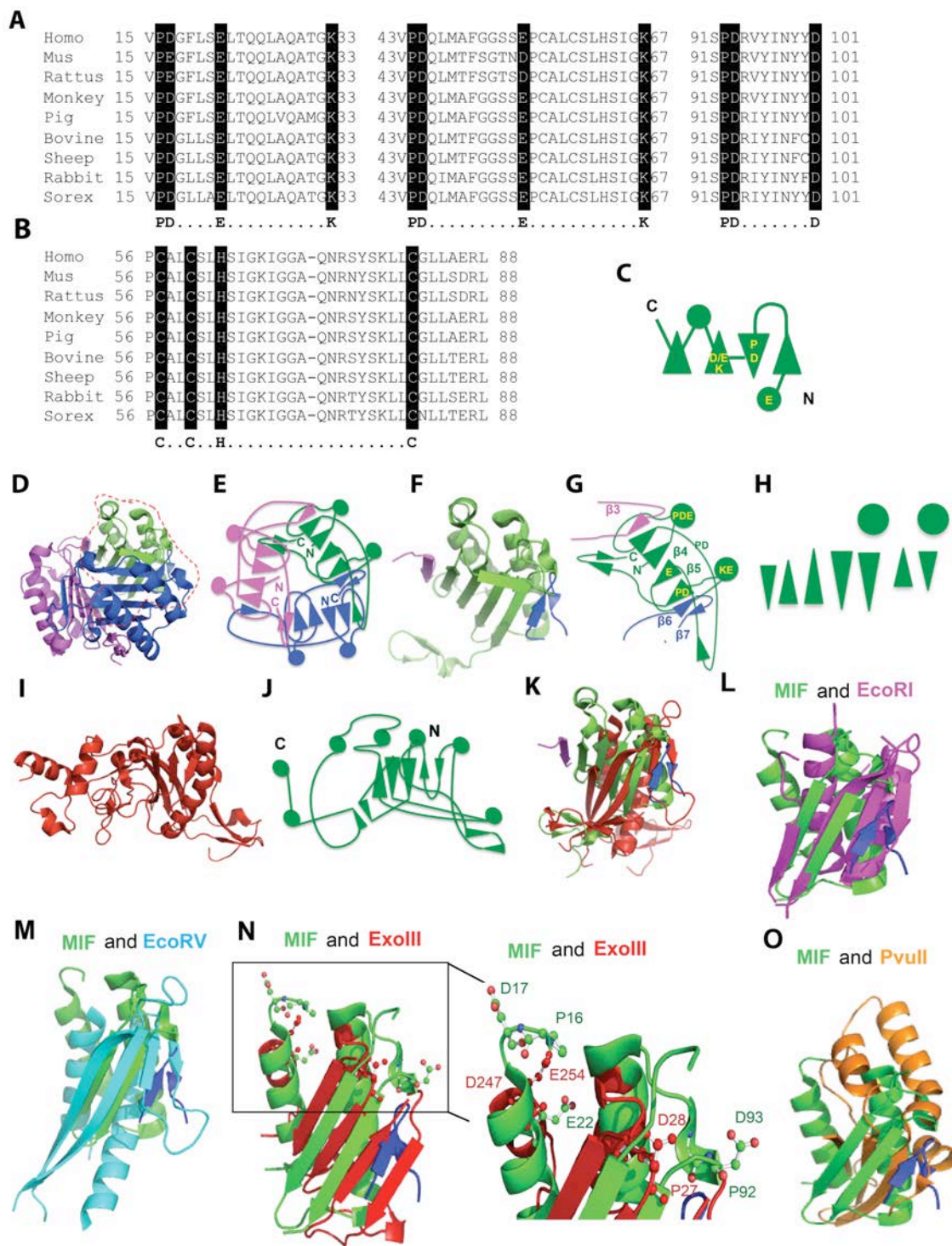


**Fig. S3**

**MIF contains PD-D/E(x)K nuclease motif.** (A) Alignments of the nuclease domains of MIF from human, mouse, rat, monkey, pig, bovine, sheep, rabbit and Sorex. (B) Alignments of the CxxCxxHx<sub>(n)</sub>C domain of MIF from human, mouse, rat, monkey, pig,

bovine, sheep, rabbit, and Sorex. **(C)** Conserved topology of the active site in PD-D/E(x)K nucleases. Image modified from Kosinski et al., (19). The alpha helices are shown as circles and beta strands are shown as triangles. The orientations of the beta-strands indicate parallel or antiparallel. **(D)** Crystal structure of MIF trimer (pdb:1GD0). Each monomer is indicated by a different color. **(E)** Topology of MIF trimer illustrating the orientations of the various domains similar to PD-D/E(x)K motif. **(F)** Crystal structure of the MIF monomer containing the PD-D/E(x)K domain derived from the trimer (broken red line in **D**) by hiding two of the monomers. **(G)** Topology of a MIF monomer in the MIF trimer. **(H)** Illustration that each monomer has a PD-D/E(x)K domain. The PD-D/E(x)K motif is made of two parallel  $\beta$ -strands ( $\beta$ 4 and  $\beta$ 5) from one monomer and two anti-parallel strands ( $\beta$ 6 and  $\beta$ 7) from the adjacent monomer. **(I)** A schematic diagram of the similarity in topology of the MIF monomer in the MIF trimer and EcoRV illustrating similar orientations of the various domains in their nuclease domains. The alpha helices are shown as circles and beta strands are shown as triangles. **(J)** Topology of EcoRV monomer. **(K)** Alignment of MIF monomer in the MIF trimer and EcoRV monomer (red). **(L-O)** Alignments of PD-D/E(x)K motif in MIF and other well known nucleases including EcoRI (magenta, pdb: 1QC9), EcoRV (light blue, pdb: 1SX8), ExoIII (red, pdb: 1AK0), and PvuII (orange, pdb 1PVU). All five motifs show similar orientations of the four beta strands in the beta-sheet against the alpha helices as observed in a typical PD-D/E(x)K motif active site.

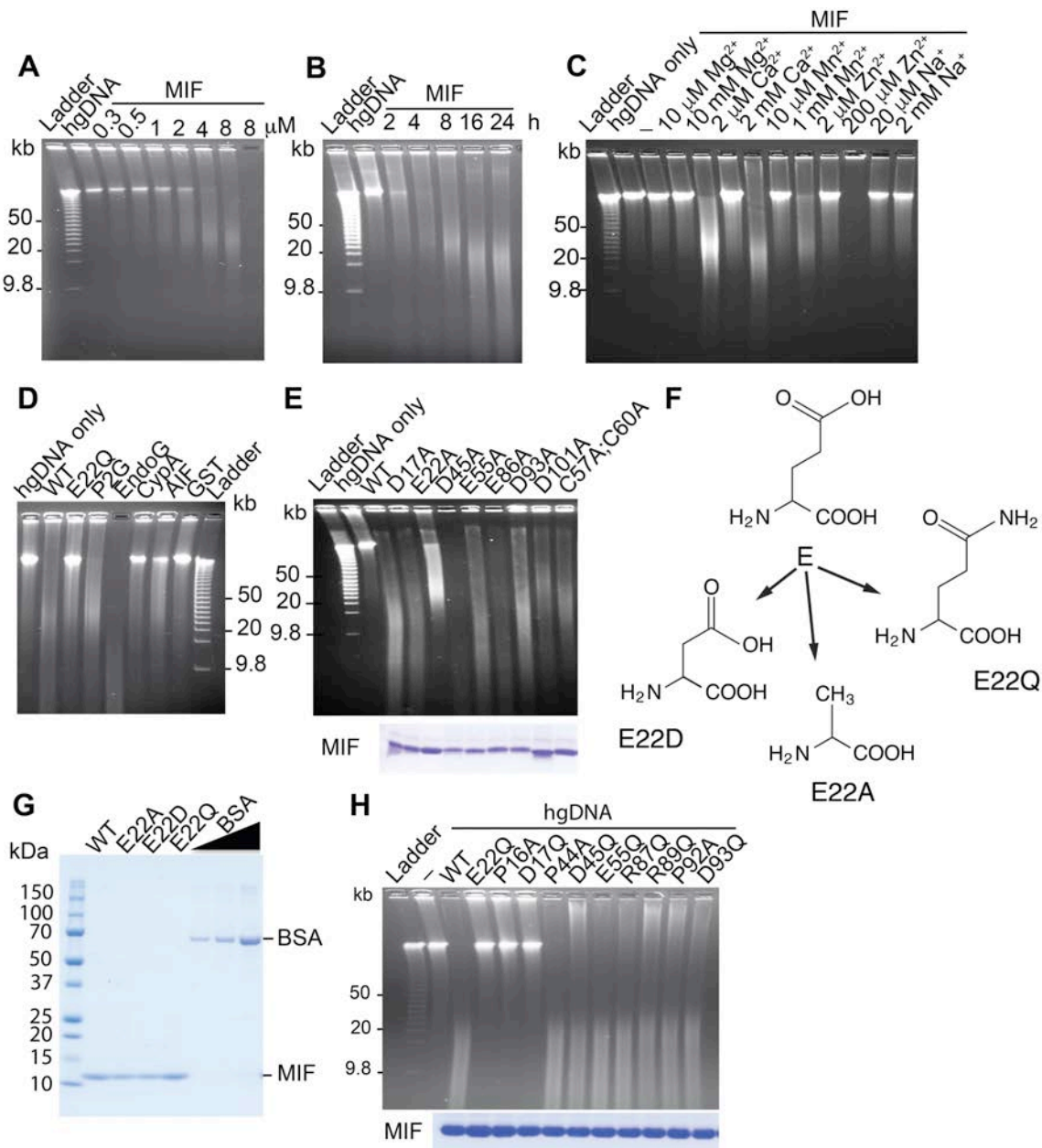


**Fig. S4.**

**MIF is a nuclease.** **(A)** Concentration-dependence of MIF incubation with human genomic DNA (hgDNA, 200 ng) in Tris-HCl buffer pH 7.0 containing 10 mM MgCl<sub>2</sub> at 37°C for 4 hours. **(B)** Time course of MIF incubation (4 μM) with hgDNA in the Tris-HCl buffer pH 7.0 containing 10 mM MgCl<sub>2</sub> at 37°C. **(C)** MIF (8 μM) incubation with hgDNA in the Tris-HCl pH 7.0 buffer with different ions as indicated at 37°C for 4 hours. **(D)** *In vitro* pulse-field gel electrophoresis-nuclease assay with purified proteins (4 μM) using human genomic DNA as the substrate. **(E)** *In vitro* pulse-field gel electrophoresis-nuclease assay with different purified MIF mutants (see Fig. 1D for illustration of MIF's amino acid sequence) using hgDNA in the Tris-HCl buffer pH 7.0 containing 10 mM MgCl<sub>2</sub> at 37°C for 4 hours. Coomassie blue staining of purified MIF WT protein and MIF mutants are shown (lower panel). **(F)** Mutation of the glutamate

residue into glutamine, aspartate and alanine. (G) Coomassie blue staining of purified MIF WT protein and MIF mutants. (H) *In vitro* pulse-field gel electrophoresis-nuclease assay with different purified MIF mutants (see Fig. 1D for illustration of mutations) using hgDNA in the Tris-HCl buffer pH 7.0 containing 10 mM MgCl<sub>2</sub> at 37°C for 4 hours. Coomassie blue staining of purified MIF WT protein and MIF mutants are shown (lower panel). The experiments were repeated using MIF protein purified in 3 independent preparations.

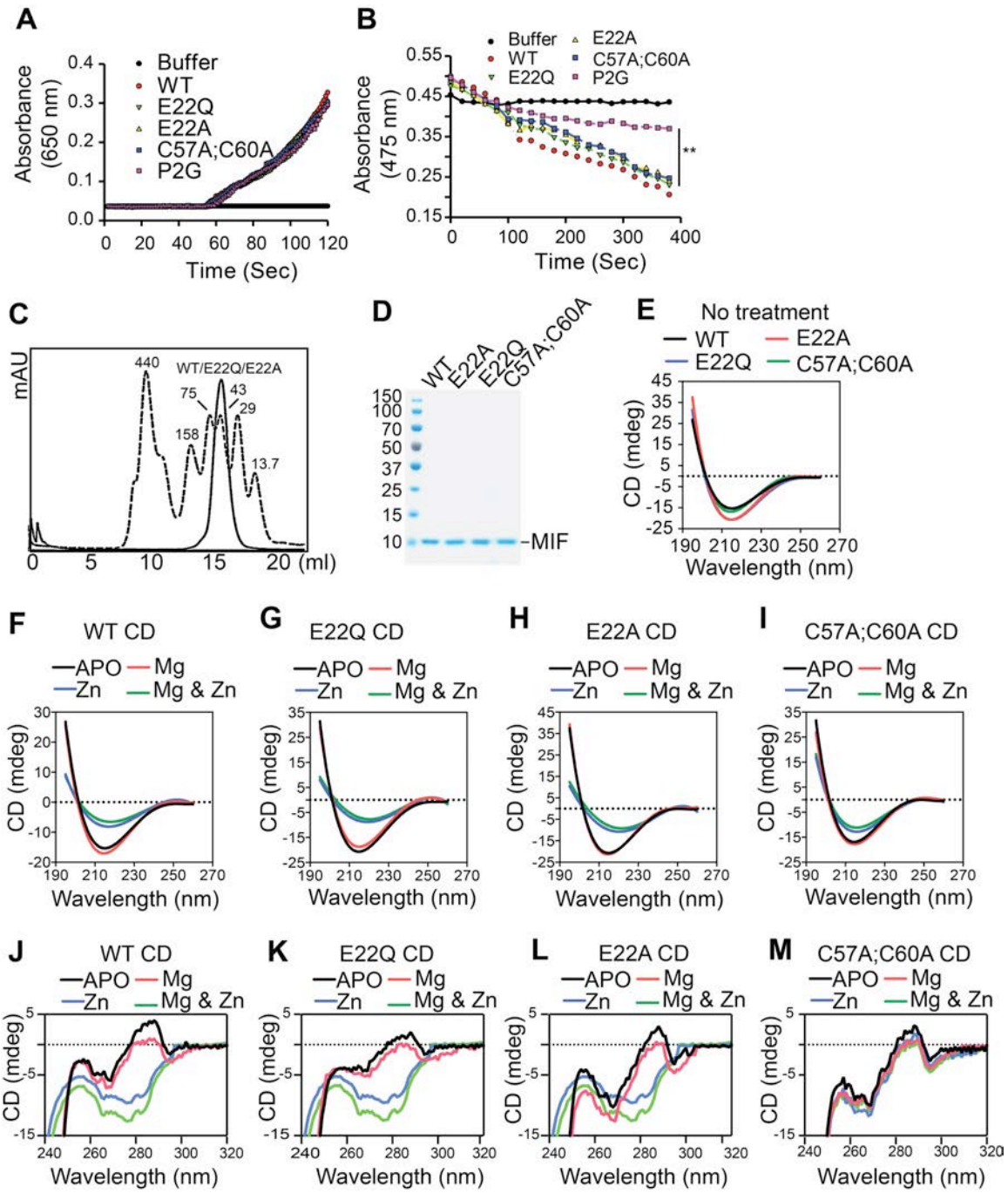


**Fig. S5.**

**Effects of MIF mutation on protein folding and enzyme activities.**

(A) Oxidoreductase activity of MIF proteins. (B) Tautomerase activity of MIF proteins. Means  $\pm$  SEM are shown in B and C. \*\* $P < 0.01$ , one-way ANOVA. (C) The FPLC profile of MIF proteins (wild type, E22Q and E22A) (solid line) and protein standard (broken line). (D) Coomassie blue staining of MIF fractions from the FPLC. (E-M) UV-CD analyses of purified MIF recombinant proteins in presence and absence of magnesium chloride (Mg) and/or zinc chloride (Zn). The experiments were replicated 3 times using MIF purified from 3 independent preparations.

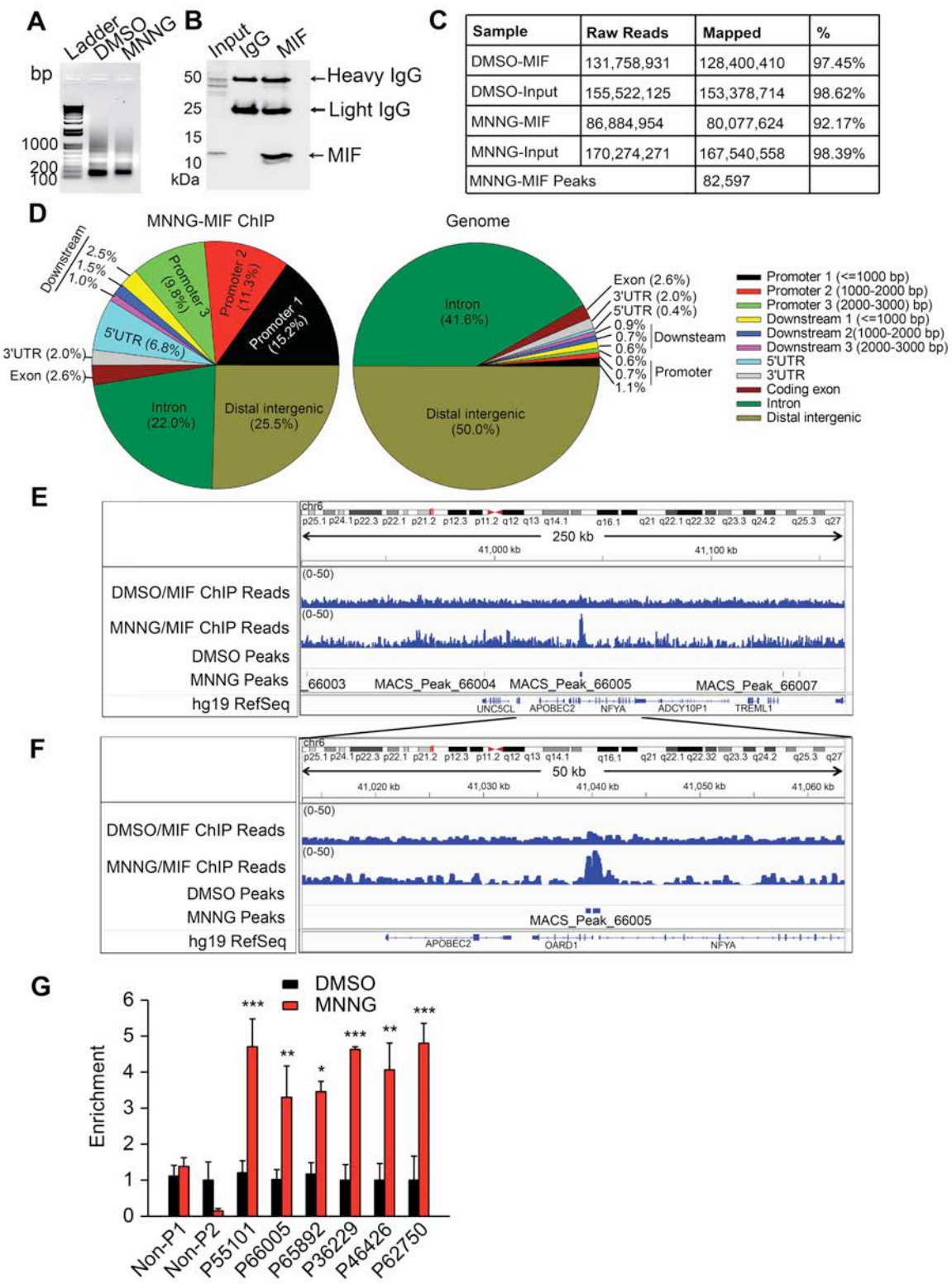


**Fig. S6.**

**Characterization of MIF-DNA binding by ChIP-seq.** (A) Sonicated fragments of chromatin are in the range of 100-200 bp for ChIP-seq in the DMSO and MNNG treated

cells. **(B)** Representative immunoblot images of MIF ChIP. **(C)** Number and coverage of the reads from four different libraries including DNA inputs and MIF ChIP samples prepared from DMSO or MNNG (50 µM) treated cells. **(D)** MIF ChIP-peak distribution across different genomic regions in MNNG treated cells. The pie chart shows that MIF tends to bind to promoters of genes (about 36 % of ChIP regions are in promoters). **(E-F)** Representative IGV visualization of MIF enrichment on the genome shown in two different chromosome window sizes. The top two lines show the tdf file of ChIP-seq data from DMSO and MNNG treated cells. The third and fourth lines show the bed files for DMSO and MNNG treated samples. The peaks were only observed in MNNG treated samples, but not in DMSO treated samples. The last line indicates the hg19 reference genes. **(G)** MIF chromatin enrichment in DMSO and MNNG treated cells confirmed by qPCR with Non-P (non peak regions), P55101, P66005, P65892, P36229, P46426 and P62750 (peak regions).

**A**

#1	-----CTCAGCCTCCCAAGTAGCTGGGATTACAGG-----
#2	CAAGCCATCCCTNCCANCTCAGCCNCCA-----
#3	-----TGGGATTACAGGCCTGAGGCCACCACGCC

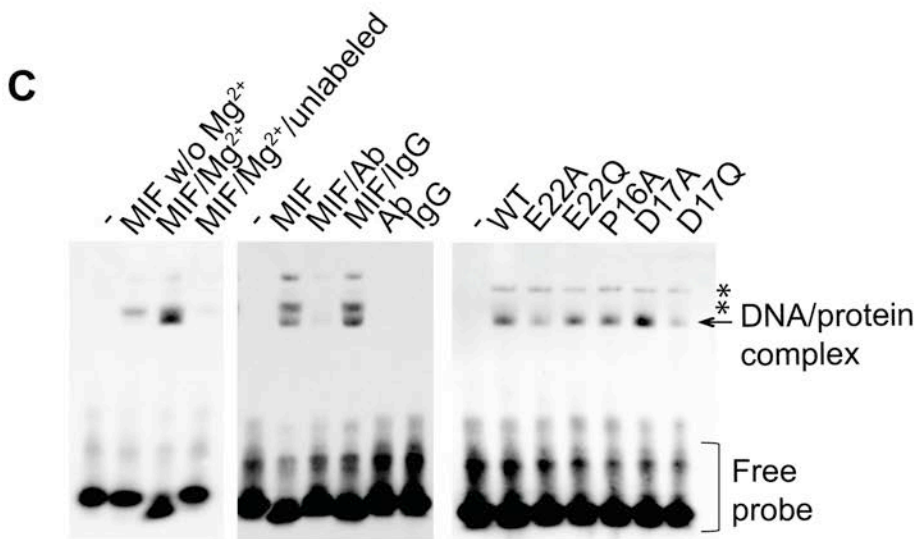
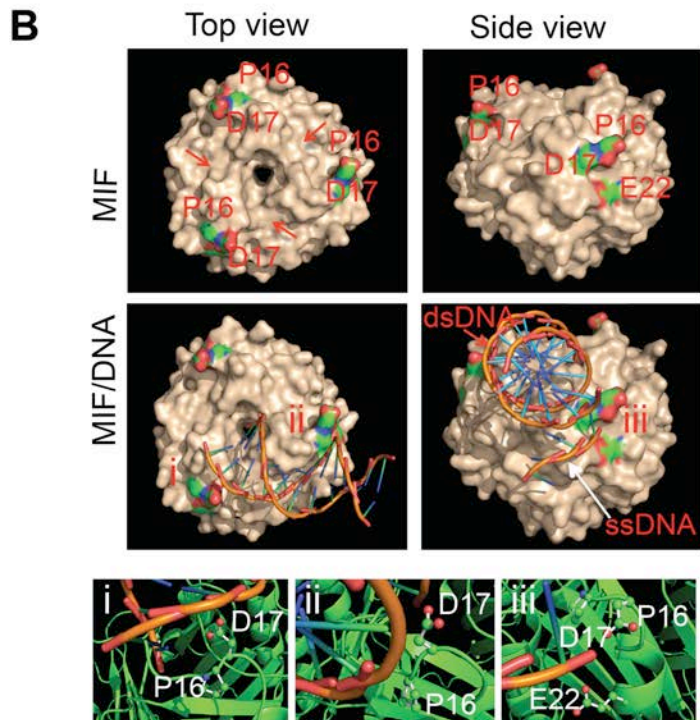
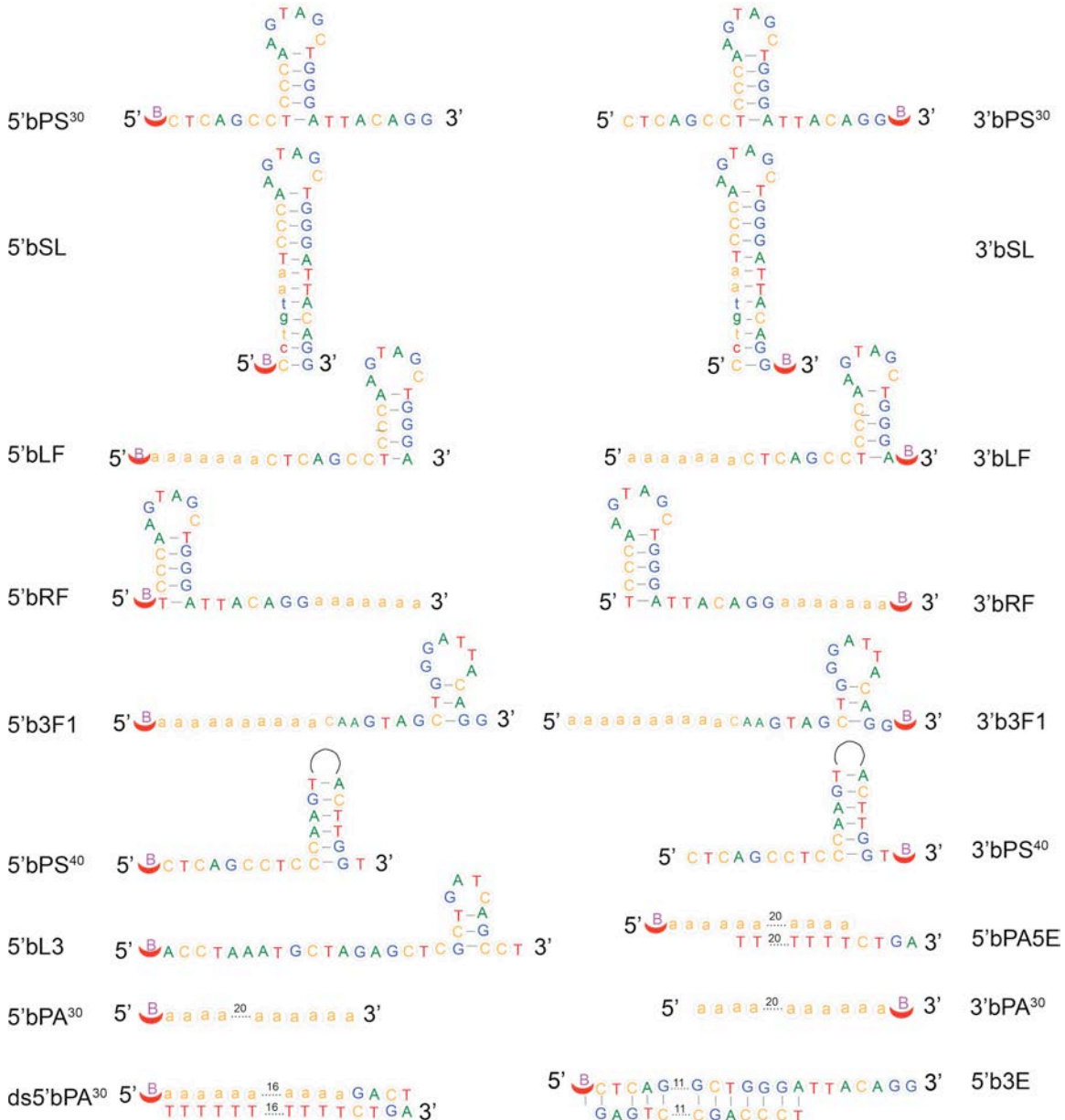


**Fig. S7.**

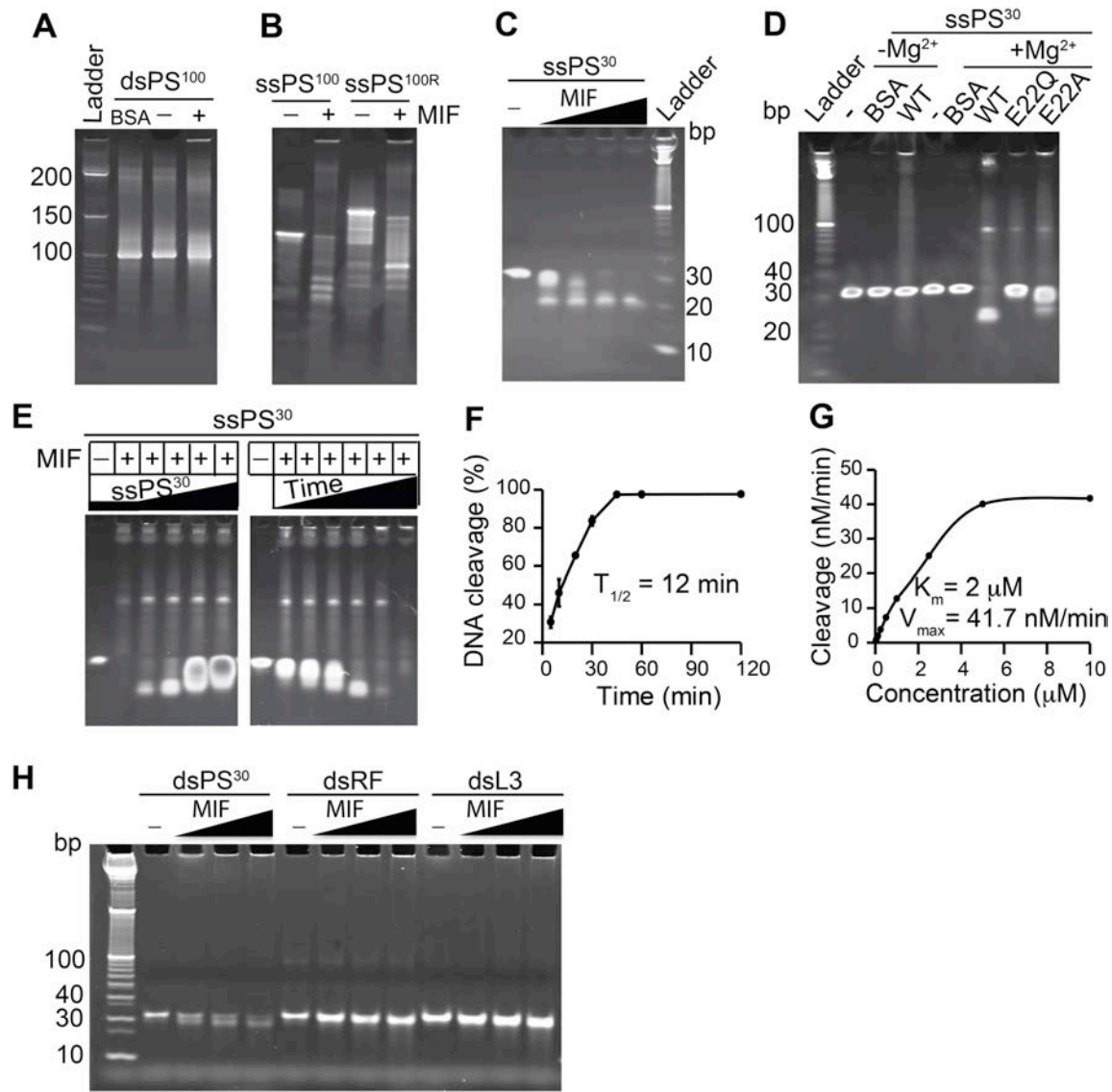
**MIF binds to single stranded DNA.** (A) Alignment of MIF DNA binding motif. (B) Images of MIF trimer (PDB accession 1FIM) surface showing a groove/binding pocket (arrows) (Top panel). Models of MIF trimer with dsDNA in the groove (Middle panel). Right image in the middle panel shows the side view of the overlay of MIF-dsDNA (PDB accession 1BNA) with MIF-ssDNA (PDB accession 2RPD) models. i-iii, Cartoon

images showing residues P16 and D17 close to dsDNA and ssDNA whereas E22 is close to the ssDNA but not the dsDNA. **(C)** Binding of MIF to the single strand 5' biotin-labeled DNA binding motif (PS<sup>30</sup>) as determined by EMSA. Left panel, binding of MIF in the presence or absence of Mg<sup>2+</sup>. Middle panel, binding of MIF in the presence of MIF antibody and controls. Right panel, binding of MIF in comparison to MIF mutants. Arrow indicates DNA/MIF protein complex. Asterix (\*) indicates nonspecific bands.

Experiments were replicated for 4 times using MIF protein purified from 3 independent preparations.

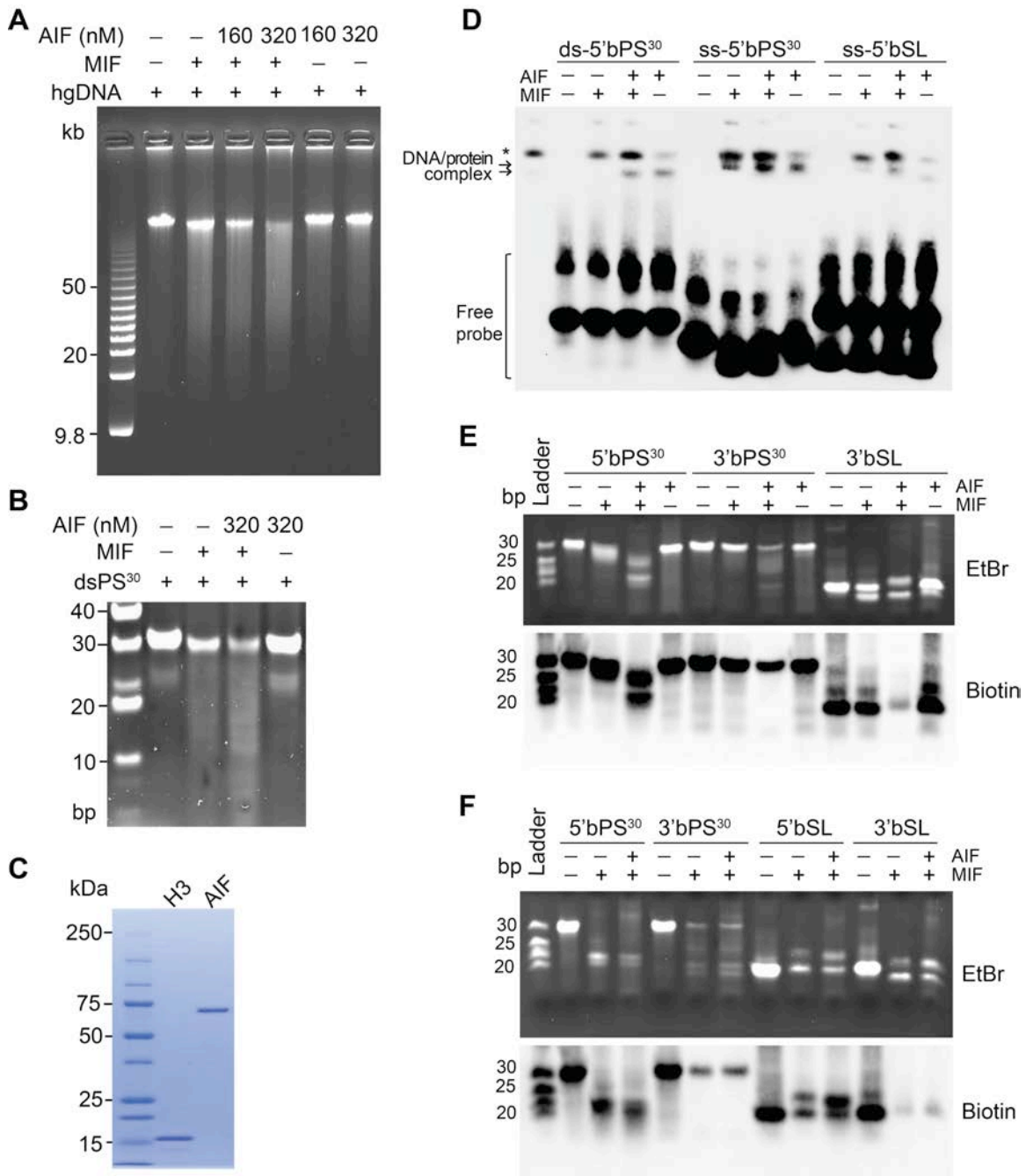


**Fig. S8.**  
**Secondary structures of different biotin-labeled DNA substrates used in binding and cleavage assays.**



**Fig. S9.**

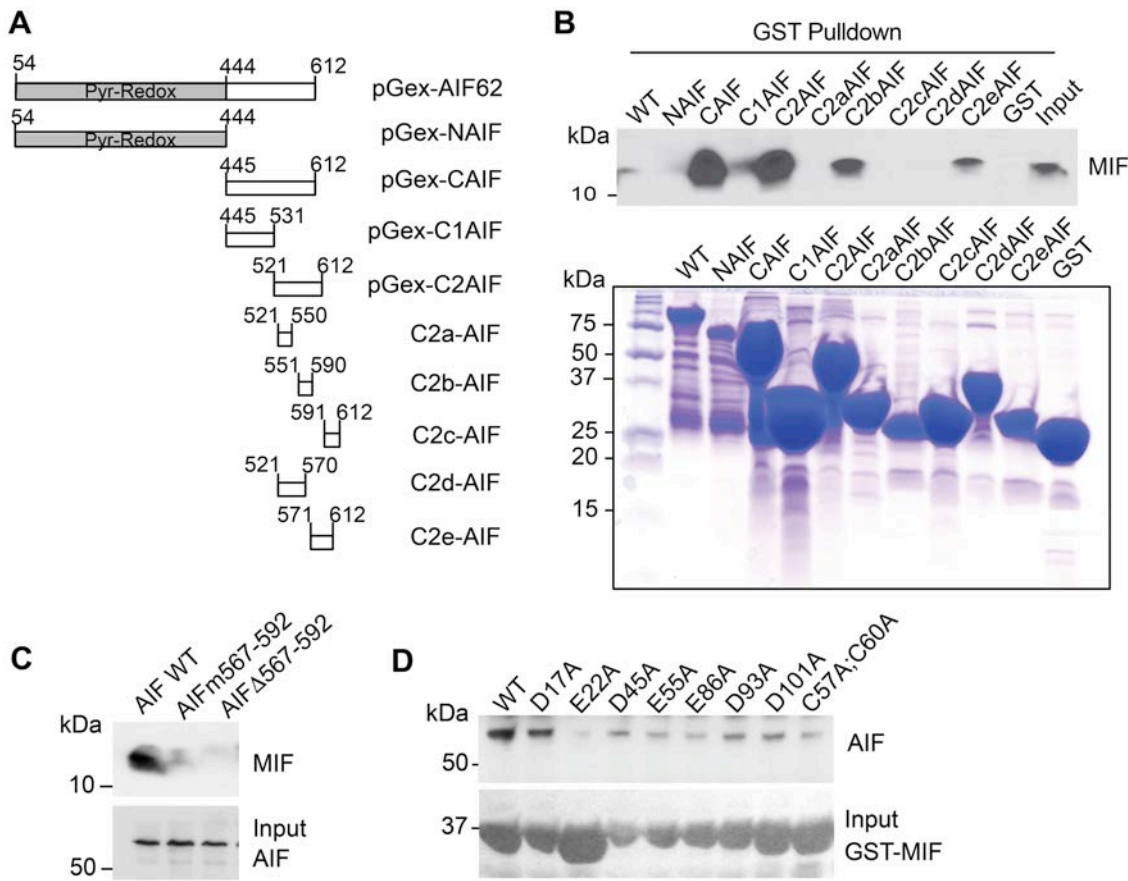
**MIF cleaves stem loop ssDNA with structure-specific nuclease activity.** (A) MIF (2  $\mu\text{M}$ ) nuclease assay using dsPS<sup>100</sup> (1  $\mu\text{M}$ ) as substrate. (B) MIF (2  $\mu\text{M}$ ) nuclease assay using ssPS<sup>100</sup> (1  $\mu\text{M}$ ) and its complementary strand ssPS<sup>100R</sup> (1  $\mu\text{M}$ ) as substrates. (C) The cleavage of ssPS30 (1  $\mu\text{M}$ ) by different concentrations of MIF (0.5, 1, 2 and 4  $\mu\text{M}$ ). (D) Nuclease assay of MIF (2  $\mu\text{M}$ ) and its mutants (2  $\mu\text{M}$ ) using ssPS<sup>30</sup> (1  $\mu\text{M}$ ) as substrate in the presence or absence Mg<sup>2+</sup>. (E-G) MIF (2  $\mu\text{M}$ ) cleaves ssPS<sup>30</sup> in a concentration (0.025, 0.05, 0.5, 2.5, 5  $\mu\text{M}$ )- and time (10, 20, 30 min and 1, 2, and 4h)-dependent manner. (H) Nuclease activity of MIF (2, 4, 8  $\mu\text{M}$ ) on dsPS<sup>30</sup> (0.2  $\mu\text{M}$ ), its sequence related substrate-dsRF (0.2  $\mu\text{M}$ ) and non-related substrate-dsL3 (0.2  $\mu\text{M}$ ). (I-J) Effects of AIF on MIF (0.5  $\mu\text{M}$ ) nuclease activity using (I) human genomic DNA 200 ng/reaction and (J) dsPS<sup>30</sup> (0.2  $\mu\text{M}$ ) as substrates. (K) Coomassie blue staining of purified AIF protein with commercial histone H3 protein as the control.



**Fig. S10.**

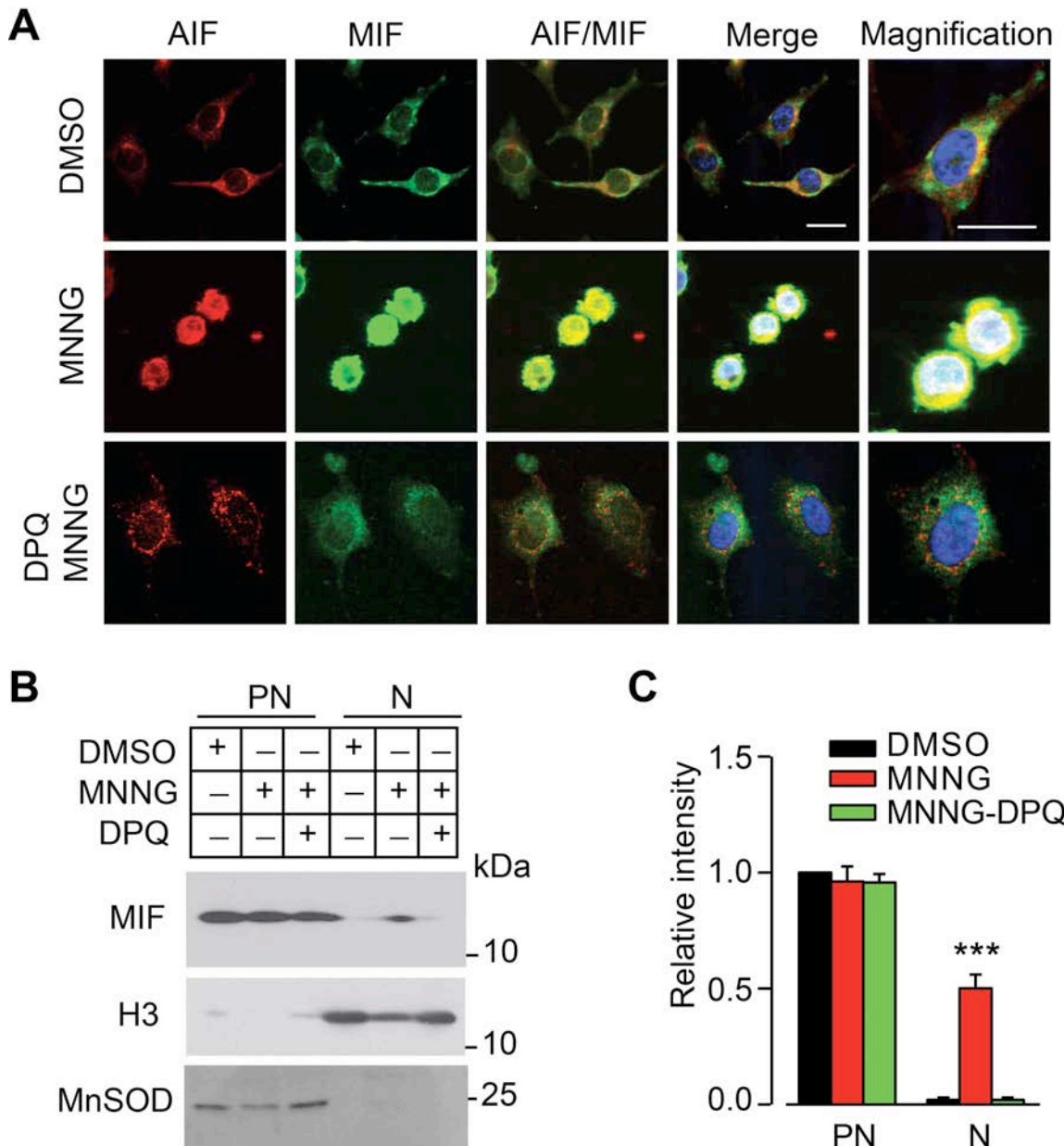
**Effects of AIF on MIF's binding and nuclease activities on double and single stranded DNAs. (A-B)** Effects of AIF on MIF (0.5  $\mu$ M) nuclease activity using (A) human genomic DNA 200 ng/reaction and (B) dsPS<sup>30</sup> (0.2  $\mu$ M) as substrates. (C) Coomassie blue staining of purified AIF protein with commercial histone H3 protein as the control. (D) Effects of AIF on MIF (0.5  $\mu$ M) binding to ds-5'bPS<sup>30</sup>, ss-5'bPS<sup>30</sup> and ss-5'bSL (10 nM). Arrows indicate DNA/protein complex. Star indicates nonspecific band. (E) Effects of AIF on MIF (0.5  $\mu$ M) nuclease activity using single stranded

$5' bPS^{30}$ ,  $3' bPS^{30}$ ,  $3' bSL$  ( $1 \mu M$ ) as substrates. **(F)** Effects of AIF on MIF ( $4 \mu M$ ) nuclease activity using single stranded  $5' bPS^{30}$ ,  $3' bPS^{30}$ ,  $5' bSL$  and  $3' bSL$  ( $1 \mu M$ ) as substrates.



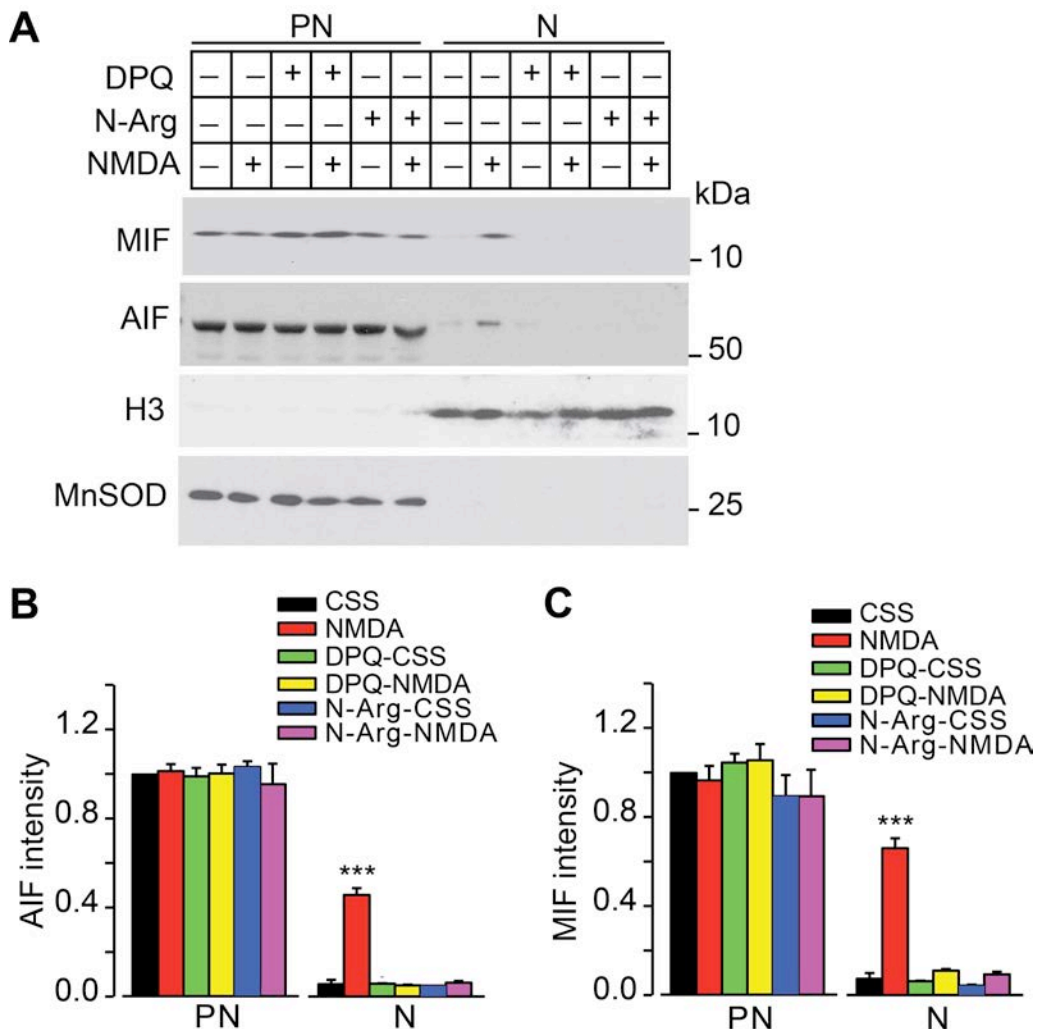
**Fig. S11.**

**MIF interacts with AIF.** (A) Schematic representation of the GST-AIF truncated proteins used in the binding assays. (B) GST pull-down assays visualized by western blot using an anti-MIF antibody (upper panel). Coomassie blue staining of GST fusion AIF truncated proteins used in the pull-down experiments (lower panel). (C) Pull-down assay of AIF mutants visualized by western blot using an anti-MIF antibody. AIFm567-592, amino acids 567-592 mutated into poly Alanine; AIFΔ567-592, amino acids 567-592 deletion. (D) GST-MIF and its variants on glutathione beads pulled down AIF protein. The experiments were replicated in 3 independent trials.



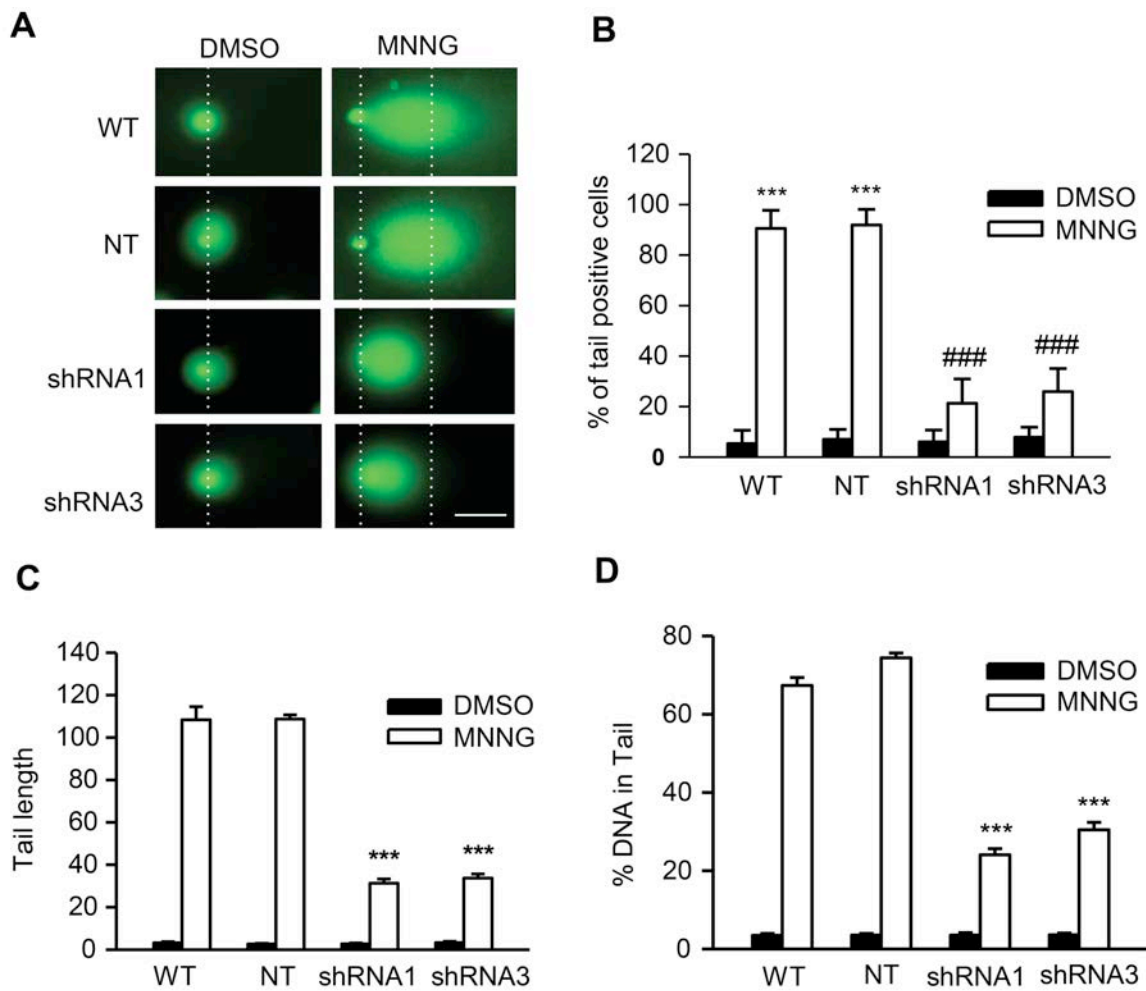
**Fig. S12.**

**MIF and AIF and cotranslocate to the nucleus in HeLa cells.** (A) Images of nuclear translocation of AIF and MIF after MNNG treatment in the presence or absence the PARP inhibitor, DPQ (30  $\mu$ M) in HeLa cells. Scale bar, 20  $\mu$ m. The yellow color in the AIF and MIF merged images shows the nuclear translocation of AIF and MIF. The white color in the merged images indicates the overlay of AIF, MIF and DAPI, showing the nuclear translocation of AIF and MIF. (B) Immunoblots of subcellular fractionation of MIF translocation to the nucleus after MNNG treatment in the presence or absence the PARP inhibitor, DPQ (30  $\mu$ M) in HeLa cells. PN, post-nuclear fraction; N, nuclear fraction. (C) Quantification of nuclear translocation of MIF after MNNG treatment in the presence or absence the PARP inhibitor, DPQ (30  $\mu$ M) in HeLa cells. \*\*\* $P < 0.001$ , one-way ANOVA. The experiments were replicated in 3 independent trials.



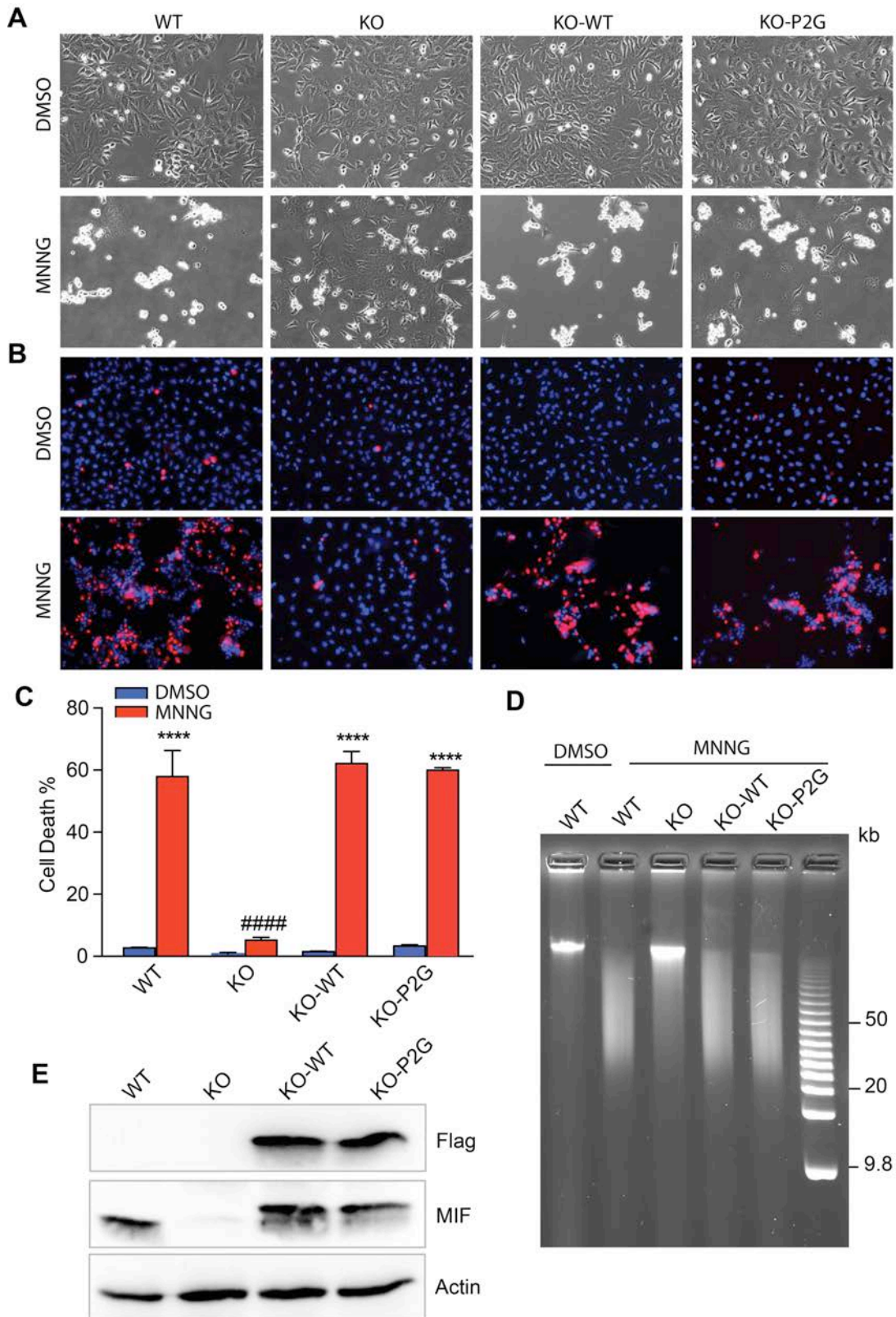
**Fig. S13.**

**MIF and AIF and cotranslocate to the nucleus in cortical neurons in a nitric oxide- and PARP- dependent manner.** (A-C) Nuclear translocation of AIF and MIF after NMDA treatment in the presence or absence of the PARP inhibitor DPQ or NOS inhibitor nitro-arginine (N-Arg, 100  $\mu$ M) in cortical neurons, which was determined by subcellular fractionation. Intensity of MIF and AIF signal is shown in B and C. The experiments were replicated in 3 independent trials. \*\*\* $P < 0.001$ , versus the DMSO control group in the nuclear fraction, one-way ANOVA.



**Fig. S14.**

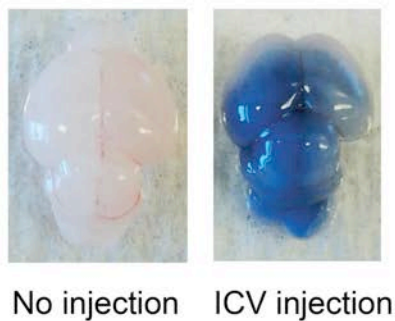
**MIF is critical for MNNG-induced DNA damage in HeLa Cells.** (A) Representative images of MNNG-caused DNA damage determined by the comet assay in wild-type (WT) HeLa cells, non-targeting (NT) shRNA or MIF shRNA lentivirus-transduced HeLa cells. Dashed lines indicate the center of the head and tail. Scale bar, 20  $\mu$ m. (B-D) Quantification of (B) % of tail positive cells, (C) tail length and (D) % of DNA in tail. Means  $\pm$  SEM are shown in B-D. \*\*\* $P < 0.001$ , versus its DMSO group, ### $P < 0.001$ , versus WT group treated with MNNG, one-way ANOVA. The experiments were replicated in 3 independent trials.



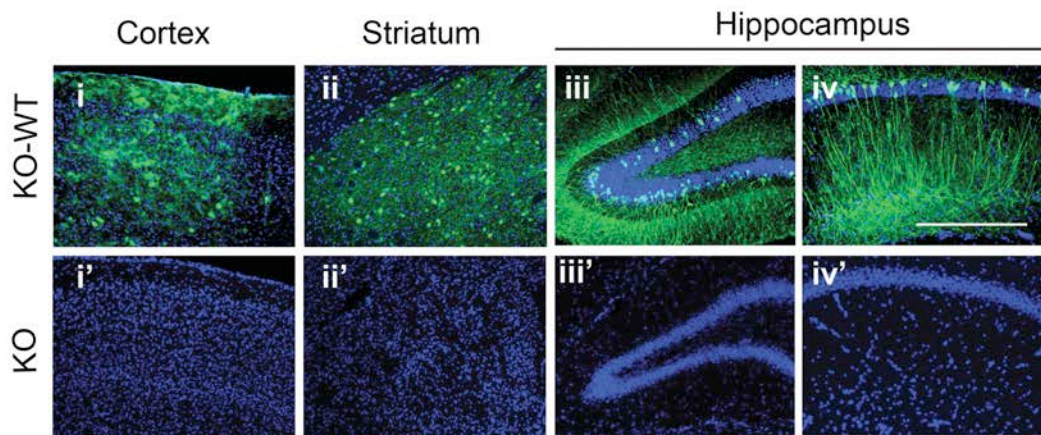
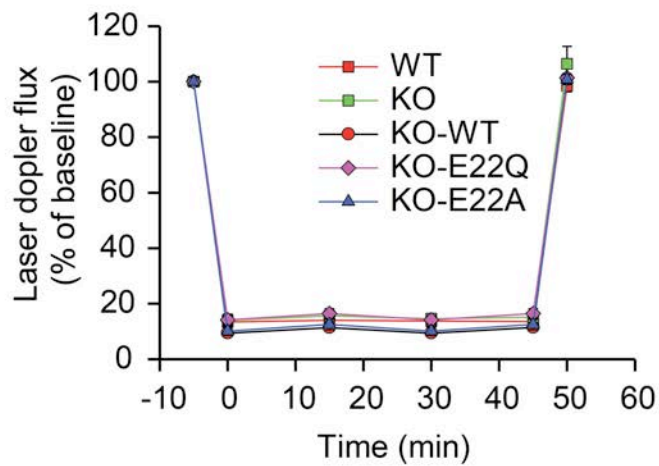
**Fig. S15.**

**Effects of MIF P2G on MNNG-induced DNA damage and parthanatos in HeLa cells.** (A-B) Representative images and (C) quantification of MNNG (50  $\mu$ M, 15 min)-

induced cytotoxicity in MIF WT, KO and KO cells expressing MIF WT or P2G. Means  $\pm$  SEM are shown \*\*\* $P < 0.0001$ , versus DMSO control, \*\*\*\* $P < 0.0001$ , versus WT group treated with MNNG, one-way ANOVA. (D) Pulse-field gel electrophoresis assay of MNNG-induced DNA damage 24 h after treatment in MIF WT, KO, and KO cells expressing MIF WT or P2G. (E) Expression of flag-tagged MIF WT and P2G in MIF KO cells.

**A**

No injection      ICV injection

**B****C****Fig.****S16.****MIF nuclease activity is required for parthanatos in stroke *in vivo*.**

(A) Intracerebroventricular (ICV) injection with trypan blue dye. (B) Representative immunostaining images of expression of AAV2-MIF WT in (i) cortex, (ii) striatum and (iii & iv) hippocampus 79 days after injection. Scale bar, 500  $\mu$ m. (C) Laser-Doppler flux measured over the lateral parietal cortex in the core of the ischemic region in WT

(n=16), MIF KO (n=12), MIF KO-WT ( $n = 11$ ), MIF KO-E22Q ( $n = 11$ ) and MIF KO-E22A ( $n = 11$ ) mice.

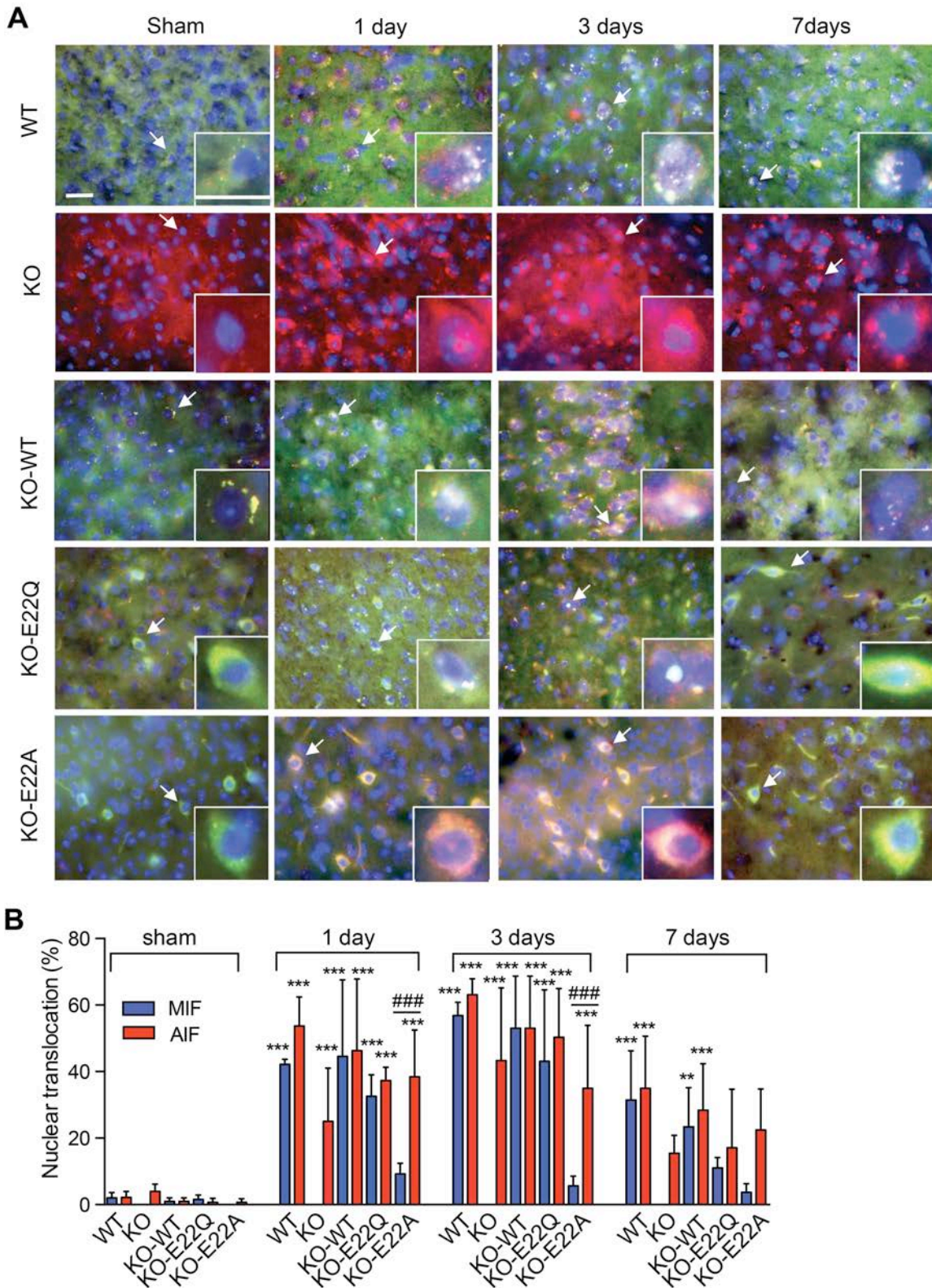


**Fig. S17.**

**MIF nuclear translocation following ischemic brain injury *in vivo*.** (A) Nuclear translocation of AIF (red) and MIF (green). (B) Quantification of nuclear translocation

of AIF (red) and MIF (green) in the penumbra 1 day, 3 days or 7 days after 45 min MCAO surgery in MIF WT, KO and KO mice which were injected with AAV2-MIF WT, E22Q or E22A. WT MCAO ( $n = 15$ ), KO MCAO ( $n = 15$ ), KO-WT MCAO ( $n = 15$ ), KO-E22Q MCAO ( $n = 15$ ), KO-E22A MCAO ( $n = 15$ ). Means  $\pm$  SEM are shown. \*\*\* $P < 0.001$  versus its sham group, # $P < 0.001$ , MIF nuclear translocation versus AIF nuclear translocation under the same condition, one-way ANOVA.

**Table S1.**  
**Sequences of MIF Substrates, Templates, Primers and guide RNA targets.**

Name	Sequence
PS <sup>100F</sup>	5'ACCTAAATGCTAGAGCTCGCTGATCAGCCTCGACTCTCAGCCTCCCAAGTAGC TGGGATTACAGGTAAACTGGTCTGACAGTTACCAATGCTTAATGAG3'
PS <sup>100R</sup>	5'CTCATTAAGCATTGGTAACTGTCAGACCAAGTTACCTGTAATCCCAGCTACTT GGGAGGCTGAGAGTCGAGGCTGATCAGCGAGCTCTAGCATTAGGT3'
PS <sup>30</sup>	5'CTCAGCCTCCCAAGTAGCTGGGATTACAGG3'
SL	5'CCTGTAATCCCAAGTAGCTGGGATTACAGG3'
LF	5'AAAAAAAACTCAGCCTCCCAAGTAGCTGGGA3'
RF	5'TCCAAGTAGCTGGGATTACAGGAAAAAAA3'
PA <sup>30</sup>	5'AAAAAAAAAAAAAAAAAAAAAAAAAAAAA3'
	5'CTCAGCCTCCCAAGTAGCTGGGATTACAGG3'
3E	5'TCCCAGCTACTGGGAGGCTGAG3'
PS <sup>40</sup>	5'CTCAGCCTCCCAAGTAGCTGGGATTACAGGTAACCTGGT3';
3F1	5'AAAAAAAACAAGTAGCTGGGATTACAGG3'
L3	5'ACCTAAATGCTAGAGCTCGCTGATCAGCCT3'
hMIFshRNA1	5'TGCTGTTGACAGTGAGCGCTCATCGTAAACACCAACGTGCTAGTGAAGCCACA GATGTAGCACGTTGGTTACGATGAATGCCTACTGCCCTCGGA3'
hMIFshRNA2	5'TGCTGTTGACAGTGAGCGACGCGCAGAACCGCTCTACAGTAGTGAAGCCAC AGATGTACTGTAGGAGCGGTTCTGCGCGCTGCCTACTGCCCTCGGA3'
hMIFshRNA3	5'TGCTGTTGACAGTGAGCGAAGGGCTACATCAACTATTACTAGTGAAGCCACA GATGTAGTAATAGTTGATGTAGACCCGTGCCTACTGCCCTCGGA3'
mMIFshRNA1	5'TGCTGTTGACAGTGAGCGCTCATCGTAACACCAATGTTCTAGTGAAGCCACA GATGTAGAACATTGGTGTTCACGATGAATGCCTACTGCCCTCGGA3'
mMIFshRNA2	5'TGCTGTTGACAGTGAGCGAGCAGTCACGTGGTCCCGGACTAGTGAAGCCAC AGATGTAGTCCGGGACCACGTGCACTGCGTGCCTACTGCCCTCGGA3'
mMIFshRNA3	5'TGCTGTTGACAGTGAGCGACGGGCTACATCAACTATTACTAGTGAAGCCACA GATGTAGTAATAGTTGATGTAGACCCGGTGCCTACTGCCCTCGGA3'
AfshRNA1	5'TGCTGTTGACAGTGAGCGCGAACCGGCTTCCAGCTACAGTAGTGAAGCCAC AGATGTACTGTAGCTGGAAGCCGGTCTGCCTACTGCCCTCGGA3'
WT-mMIF-fw	5'CGGGATCCGCCACCATGCCATGCTATGTTCATCGTGAAC3'
WT-mMIF-re	5'CGGAATTCTCAAGCGAAGGTGGAACCGT3'
Rsh1-mMIF-fw	5'CACCATGCCTATGTTATTGTCATAACGAACGTACCCGCGCCTCCGTG3'
Rsh1-mMIF-re	5'CACGGAGGC CGGGGTACGTTCGTATTGACAATAAACATAGGCATGGT3'
Rsh3-mMIF-fw	5'GCACATCAGCCGGACCGCGTGTATATTAAATTACTATGACATGAACGCTGCC3'
Rsh3-mMIF-re	5'GGCAGCGTTCATGTCATAGTAATTAAATACACGCGGTCCGGCTGATGTG3'
hMIF P2G Fw	5'GGGATCCCCGGAATTCggGATGTTCATCGTAAACACC3'
hMIF P2G Re	5'GGTGTTCACGATGAACATCCGAATTCCGGGGATCCC3'
P16A-hMIF-fw	5'CCTCCGTGGCGGACGGGTTCTC3'
P16A-hMIF-re	5'GAACCCGTCCGCCACGGAGG3'
D17A-hMIF-fw	5'CGGCCCTCCGTGCCGGCGGGTTCTCTCC3'
D17A-hMIF-re	5'GGAGAGGAACCCGGCCGGCACGGAGGCGCG3'
D17Q-hMIF-fw	5'CCGTGCCGAAGGGTTCTC3'
D17Q-hMIF-re	5'GAGGAACCCCTGCGGCACGG3'
E22A-hMIF-fw	5'GGGTT CCTCTCCCGCGCTACCCAGCAGCTG3'
E22A-hMIF-re	5'CAGCTGCTGGGTGAGCGCGGAGAGGAACCC3'
E22Q-hMIF-fw	5'GGGTT CCTCTCCAGCTACCCAGCAGCTG3'
E22Q-hMIF-re	5'CAGCTGCTGGGTGAGCTGGGAGAGGAACCC3'
E22D-hMIF-fw	5'GGGTT CCTCTCCGACCTCACCCAGCAGCTG3'

E22D-hMIF-re	5'CAGCTGCTGGGTGAGGTCGGAGAGGAACCC3'
P44A-hMIF-fw	5'GTGCACGTGGTCGCCGACCA3'
P44A-hMIF-re	5'CATGAGCTGGTCCCGCAGCTCATGGCCTTC3'
D45A-hMIF-fw	5'GCACGTGGTCCCGGCCAGCTCATGGCCTTC3'
D45A-hMIF-re	5'GAAGGCCATGAGCTGGGCCGGACCACGTGC3'
D45Q-hMIF-fw	5'GTGGTCCCAGCACAGCTCAT3'
D45Q-hMIF-re	5'CCATGAGCTGGTGCAGGACC3'
E55A-hMIF-fw2	5'CTTCGGCGGCTCCAGCGCGCCGTGCGCGCTTG3'
E55A-hMIF-re2	5'CAGAGCGCGCACGGCGCGCTGGAGGCCGCGAAG3'
E55D-hMIF-fw	5'CTCCAGCCAGCGTGCAGCGC3'
E55D-hMIF-re	5'GCGCGCACGGCTGGCTGGAG3'
E86A-hMIF-fw	5'GGCCTGCTGGCCGCGCGCTGCGCATCAGC3'
E86A-hMIF-re	5'GCTGATGCGCAGCGCGCGCCAGCAGGCC3'
R87Q-hMIF-fw	5'GCTGCCGAGCAACTGCGCATCAGC3'
R87Q-hMIF-re	5'CTGATGCGCAGTTGCTGGCCAGC3'
R89Q-hMIF-fw	5'CCGAGCGCCTGCAAATCAGC3'
R89Q-hMIF-re	5'GCTGATGCGCAGTTGCTGG3'
P92A-hMIF-fw	5'GCGCATCAGCGCGACAGGG3'
P92A-hMIF-re	5'CCCTGTCCCGCCTGATGCGC3'
D93A-hMIF-fw	5'CTGCGCATCAGCCCAGGCCAGGGTCTACATCAAC3'
D93A-hMIF-re	5'GTTGATGTAGACCCCTGGCCGGCTGATGCGCAG3'
D93Q-hMIF-fw	5'CAGCCCGAAAGGGTCTACA3'
D93Q-hMIF-re	5'TGTAGACCCTTGCGGGCTG3'
D101A-hMIF-fw	5'CATCAACTATTACGCCATGAACGCCG3'
D101A-hMIF-re	5'GGCCCGCTTCATGGCGTAATAGTTGATG3'
C57A;C60AhMIFfw	5'CGGCGGCTCCAGCGAGCCGGCCGCGCTGCCAGCCTGCACAGCATCGGC3'
C57A;C60AhMIFre	5'GCCGATGCTGTGCAGGCTGGCGAGCGCGGGCTCGCTGGAGGCCGCG3'
E22D-mMIF-fw	5'GAGGGGTTCTGTCGGACCTCACCCAGCAGCTG3'
E22D-mMIF-re	5'CAGCTGCTGGGTGAGGTCGACAGAAACCCCTC3'
E22Q-mMIF-fw	5'GAGGGGTTCTGTCGCAGCTCACCCAGCAGCTG3'
E22Q-mMIF-re	5'CAGCTGCTGGGTGAGCTGCACAGAAACCCCTC3'
AAV2-mMIFfw	5'CGGATCCGCCACCATGCCATGCTATGTTCATCGT3'
AAV2-mMIFre	5'CGGAATTCTCACTGTCGTCGTCGTCCTGTAGTCAGCGAAGGTGGAACCGT3'
P2GmMIFfw	5'CCACCGGTGCCACCATGggTATGTTCATCGTGAAC3'
P2GmMIFre	5'CGGAATTCTCACTGTCGTCGTCGTCCTGTAGTCAGCGAAGGTGGAACCGT3'
hEndoG-fw	5'CGGAATTCATGCGGGCGCTGCGGGCCGGCT3'
hEndoG-re	5'CCGCTCGAGTCACTTACTGCCGCCGTGATG3'
hCypA-fw	5'CGGAATTATGGTCAACCCACCGTGTTC3'
hCypA-re	5'CCGCTCGAGTTATCGAGTTGTCCACAGTCAG3'
hMIF gRNA1	5'GAGGAACCCGTCCGGCACGG3' (target sequence)
EndoG gRNA1	5'CCGCCGCCGCCAACACCACCGC 3' (target sequence)
EndoG gRNA2	5'GGGCTGGGTGCGGGCTCGA3' (target sequence)

**Table S2.**  
**Summary of MIF substrates used for the nuclease assays.**

Name	Sequence	Loop	Loop sequence same?	Endo-Nuclease Activity	Exo-Nuclease Activity
PS <sup>30</sup>	5'Bio-CTCAGCCTCCCAAGTAGCTGGATTACAGG3'	Y	Y	Y	Y
PS <sup>40</sup>	5'Bio-CTCAGCCTCCCAAGTAGCTGGATTACAGGTAAACTGGT3'	Y	N	Y	Y
3F1	5'Bio-AAAAAAAAACAAGTAGCTGGATTACAGG3'	Y	N	Y	Y
m2	5'Bio-/CTCAGCCTCCAAAAAAAAGGATTACAGG3'	Y	N	Y	Y
m3	5'Bio-CTCAGCCTCCCAAGTAGCTGAAAAAAA3'	Y	N	Y	Y
m4	5'Bio-CTCAGCCAAAAAATAGCTGGATTACAGG3'	Y	N	Y	Y
m5	5'Bio-CTCAGCCTCCCAAAAAAAAGGATTACAGG3'	Y	N	Y	Y
m6	5'Bio-CTCAAAAAACAAGTAGCTGGATTACAGG3'	Y	N	Y	Y
m7	5'Bio-AAAAGCCTCCCAAGTAGCTGGATTACAGG3'	Y	Y	Y	Y
m8	5'Bio-CTCAAAATCCCAAAAAAAAGGATTACAGG3'	Y	N	Y	Y
m9	5'Bio-CAAGTAGCTGCTCAGCCTCCGGATTACAGG3'	Y	N	Y	Y
m10	5'Bio-CTCAGCCTCCGGATTACAGGCAAGTAGCTG3'	Y	N	Y	Y
m11	5'Bio-CTCAGCCTCCCAAGTAAAAGGATTACAGG3'	Y	N	Y	Y
m12	5'Bio-CTCAGCCTCCCAAGTAAATGGGATTACAGG3'	Y	N	Y	Y
m14	5'Bio-CTCAGCCTCCCAAGTAaacGGGATTACAGG3'	Y	N	Y	Y
m15	5'Bio-CTCAGCCTCCCAAGTAGCaGGGATTACAGG3'	Y	N	Y	Y
m16	5'Bio-CTCAGCCTCCttGTAGCTGGATTACAGG3'	Y	N	Y	Y
m17	5'Bio-CTCAAAATCCCAAGTAGCTGGATTACAGG3'	Y	Y	Y	Y
m18	5'Bio-CTCAattTCCCAAGTAGCTGGATTACAGG3'	Y	Y	Y	Y
SL	5'Bio-CCTGTAATCCCAAGTAGCTGGATTACAGG3'	Y	Y	N	N
LF	5'Bio-AAAAAAACTCAGCCTCCCAAGTAGCTGGGA	Y	Y	N	N
m20	5'Bio-AAAAATCTCAGCCTCCCAAGTAGCTGGAT3'	Y	N	Y	Y
RF	5'Bio-TCCCAAGTAGCTGGATTACAGGAAAAAAA3'	Y	N	Y	Y
BS2	5'Bio-TGGGATTACAGGCCTGAGCCACCACGCC3'	Y	N	Y	Y
PA <sup>30</sup>	5'Bio-AAAAAAAAAAAAAAAAAAAAAAAAAAA3'	N	--	N	Y
	5'CTCAGCCTCCCAAGTAGCTGGATTACAGG3';				
3E	5'TCCCAGCTACTTGGGAGGCTGAG3'	N	--	N	Y
L3	5'Bio-ACCTAAATGCTAGAGCTCGCTGATCAGCCT3'	Y	N	Y	Y

Note: Bio, Biotin; Y, yes; N, no.

## References and Notes

1. P. Bai, Biology of poly(ADP-ribose) polymerases: The factotums of cell maintenance. *Mol. Cell* **58**, 947 (2015).
2. A. A. Fatokun, V. L. Dawson, T. M. Dawson, Parthanatos: Mitochondrial-linked mechanisms and therapeutic opportunities. *Br. J. Pharmacol.* **171**, 2000–2016 (2014). [Medline](#) [doi:10.1111/bph.12416](https://doi.org/10.1111/bph.12416)
3. Y. Wang, V. L. Dawson, T. M. Dawson, Poly(ADP-ribose) signals to mitochondrial AIF: A key event in parthanatos. *Exp. Neurol.* **218**, 193–202 (2009). [Medline](#) [doi:10.1016/j.expneurol.2009.03.020](https://doi.org/10.1016/j.expneurol.2009.03.020)
4. P. Pacher, C. Szabo, Role of the peroxynitrite-poly(ADP-ribose) polymerase pathway in human disease. *Am. J. Pathol.* **173**, 2–13 (2008). [Medline](#) [doi:10.2353/ajpath.2008.080019](https://doi.org/10.2353/ajpath.2008.080019)
5. C. Szabó, V. L. Dawson, Role of poly(ADP-ribose) synthetase in inflammation and ischaemia-reperfusion. *Trends Pharmacol. Sci.* **19**, 287–298 (1998). [Medline](#) [doi:10.1016/S0165-6147\(98\)01193-6](https://doi.org/10.1016/S0165-6147(98)01193-6)
6. S. Martire, L. Mosca, M. d'Erme, PARP-1 involvement in neurodegeneration: A focus on Alzheimer's and Parkinson's diseases. *Mech. Ageing Dev.* **146–148**, 53–64 (2015). [Medline](#) [doi:10.1016/j.mad.2015.04.001](https://doi.org/10.1016/j.mad.2015.04.001)
7. L. Virág, A. Robaszkiewicz, J. M. Rodriguez-Vargas, F. J. Oliver, Poly(ADP-ribose) signaling in cell death. *Mol. Aspects Med.* **34**, 1153–1167 (2013). [Medline](#) [doi:10.1016/j.mam.2013.01.007](https://doi.org/10.1016/j.mam.2013.01.007)
8. H. Wang, S. W. Yu, D. W. Koh, J. Lew, C. Coombs, W. Bowers, H. J. Federoff, G. G. Poirier, T. M. Dawson, V. L. Dawson, Apoptosis-inducing factor substitutes for caspase executioners in NMDA-triggered excitotoxic neuronal death. *J. Neurosci.* **24**, 10963–10973 (2004). [Medline](#) [doi:10.1523/JNEUROSCI.3461-04.2004](https://doi.org/10.1523/JNEUROSCI.3461-04.2004)
9. Y. Wang, N. S. Kim, J. F. Haince, H. C. Kang, K. K. David, S. A. Andrabi, G. G. Poirier, V. L. Dawson, T. M. Dawson, Poly(ADP-ribose) (PAR) binding to apoptosis-inducing factor is critical for PAR polymerase-1-dependent cell death (parthanatos). *Sci. Signal.* **4**, ra20 (2011). [Medline](#) [doi:10.1126/scisignal.2000902](https://doi.org/10.1126/scisignal.2000902)
10. S. W. Yu, S. A. Andrabi, H. Wang, N. S. Kim, G. G. Poirier, T. M. Dawson, V. L. Dawson, Apoptosis-inducing factor mediates poly(ADP-ribose) (PAR) polymer-induced cell death. *Proc. Natl. Acad. Sci. U.S.A.* **103**, 18314–18319 (2006). [Medline](#) [doi:10.1073/pnas.0606528103](https://doi.org/10.1073/pnas.0606528103)
11. S. W. Yu, H. Wang, M. F. Poitras, C. Coombs, W. J. Bowers, H. J. Federoff, G. G. Poirier, T. M. Dawson, V. L. Dawson, Mediation of poly(ADP-ribose) polymerase-1-dependent cell death by apoptosis-inducing factor. *Science* **297**, 259–263 (2002). [Medline](#) [doi:10.1126/science.1072221](https://doi.org/10.1126/science.1072221)

12. X. Wang, C. Yang, J. Chai, Y. Shi, D. Xue, Mechanisms of AIF-mediated apoptotic DNA degradation in *Caenorhabditis elegans*. *Science* **298**, 1587–1592 (2002). [Medline](#) [doi:10.1126/science.1076194](#)
13. K. K. David, M. Sasaki, S. W. Yu, T. M. Dawson, V. L. Dawson, EndoG is dispensable in embryogenesis and apoptosis. *Cell Death Differ.* **13**, 1147–1155 (2006). [Medline](#) [doi:10.1038/sj.cdd.4401787](#)
14. R. A. Irvine, N. Adachi, D. K. Shibata, G. D. Cassell, K. Yu, Z. E. Karanjawala, C. L. Hsieh, M. R. Lieber, Generation and characterization of endonuclease G null mice. *Mol. Cell. Biol.* **25**, 294–302 (2005). [Medline](#) [doi:10.1128/MCB.25.1.294-302.2005](#)
15. Z. Xu, J. Zhang, K. K. David, Z. J. Yang, X. Li, T. M. Dawson, V. L. Dawson, R. C. Koehler, Endonuclease G does not play an obligatory role in poly(ADP-ribose) polymerase-dependent cell death after transient focal cerebral ischemia. *Am. J. Physiol. Regul. Integr. Comp. Physiol.* **299**, R215–R221 (2010). [Medline](#) [doi:10.1152/ajpregu.00747.2009](#)
16. S. Hu, Z. Xie, A. Onishi, X. Yu, L. Jiang, J. Lin, H. S. Rho, C. Woodard, H. Wang, J. S. Jeong, S. Long, X. He, H. Wade, S. Blackshaw, J. Qian, H. Zhu, Profiling the human protein-DNA interactome reveals ERK2 as a transcriptional repressor of interferon signaling. *Cell* **139**, 610–622 (2009). [Medline](#) [doi:10.1016/j.cell.2009.08.037](#)
17. T. Calandra, B. Echtenacher, D. L. Roy, J. Pugin, C. N. Metz, L. Hültner, D. Heumann, D. Männel, R. Bucala, M. P. Glauser, Protection from septic shock by neutralization of macrophage migration inhibitory factor. *Nat. Med.* **6**, 164–170 (2000). [Medline](#) [doi:10.1038/72262](#)
18. M. Merk, R. A. Mitchell, S. Endres, R. Bucala, D-Dopachrome tautomerase (D-DT or MIF-2): Doubling the MIF cytokine family. *Cytokine* **59**, 10–17 (2012). [Medline](#) [doi:10.1016/j.cyto.2012.03.014](#)
19. J. Kosinski, M. Feder, J. M. Bujnicki, The PD-(D/E)XK superfamily revisited: Identification of new members among proteins involved in DNA metabolism and functional predictions for domains of (hitherto) unknown function. *BMC Bioinformatics* **6**, 172 (2005). [Medline](#) [doi:10.1186/1471-2105-6-172](#)
20. K. Kratz, B. Schöpf, S. Kaden, A. Sendoel, R. Eberhard, C. Lademann, E. Cannavó, A. A. Sartori, M. O. Hengartner, J. Jiricny, Deficiency of FANCD2-associated nuclease KIAA1018/FAN1 sensitizes cells to interstrand crosslinking agents. *Cell* **142**, 77–88 (2010). [Medline](#) [doi:10.1016/j.cell.2010.06.022](#)
21. C. MacKay, A. C. Déclais, C. Lundin, A. Agostinho, A. J. Deans, T. J. MacArtney, K. Hofmann, A. Gartner, S. C. West, T. Helleday, D. M. Lilley, J. Rouse, Identification of KIAA1018/FAN1, a DNA repair nuclease recruited to DNA damage by monoubiquitinated FANCD2. *Cell* **142**, 65–76 (2010). [Medline](#) [doi:10.1016/j.cell.2010.06.021](#)
22. H. Sugimoto, M. Suzuki, A. Nakagawa, I. Tanaka, J. Nishihira, Crystal structure of macrophage migration inhibitory factor from human lymphocyte at 2.1 Å

- resolution. *FEBS Lett.* **389**, 145–148 (1996). [Medline doi:10.1016/0014-5793\(96\)00553-4](#)
23. H. W. Sun, J. Bernhagen, R. Bucala, E. Lolis, Crystal structure at 2.6-A resolution of human macrophage migration inhibitory factor. *Proc. Natl. Acad. Sci. U.S.A.* **93**, 5191–5196 (1996). [Medline doi:10.1073/pnas.93.11.5191](#)
24. M. Suzuki, H. Sugimoto, A. Nakagawa, I. Tanaka, J. Nishihira, M. Sakai, Crystal structure of the macrophage migration inhibitory factor from rat liver. *Nat. Struct. Biol.* **3**, 259–266 (1996). [Medline doi:10.1038/nsb0396-259](#)
25. M. Laganeckas, M. Margelevicius, C. Venclovas, Identification of new homologs of PD-(D/E)XK nucleases by support vector machines trained on data derived from profile-profile alignments. *Nucleic Acids Res.* **39**, 1187–1196 (2011). [Medline doi:10.1093/nar/gkq958](#)
26. K. Steczkiewicz, A. Muszewska, L. Knizewski, L. Rychlewski, K. Ginalski, Sequence, structure and functional diversity of PD-(D/E)XK phosphodiesterase superfamily. *Nucleic Acids Res.* **40**, 7016–7045 (2012). [Medline doi:10.1093/nar/gks382](#)
27. V. Pingoud, W. Wende, P. Friedhoff, M. Reuter, J. Alves, A. Jeltsch, L. Mones, M. Fuxreiter, A. Pingoud, On the divalent metal ion dependence of DNA cleavage by restriction endonucleases of the EcoRI family. *J. Mol. Biol.* **393**, 140–160 (2009). [Medline doi:10.1016/j.jmb.2009.08.011](#)
28. J. B. Lubetsky, A. Dios, J. Han, B. Aljabari, B. Ruzsicska, R. Mitchell, E. Lolis, Y. Al-Abed, The tautomerase active site of macrophage migration inhibitory factor is a potential target for discovery of novel anti-inflammatory agents. *J. Biol. Chem.* **277**, 24976–24982 (2002). [Medline doi:10.1074/jbc.M203220200](#)
29. G. Fingerle-Rowson, D. R. Kaleswarapu, C. Schlander, N. Kabgani, T. Brocks, N. Reinart, R. Busch, A. Schütz, H. Lue, X. Du, A. Liu, H. Xiong, Y. Chen, A. Nemajerova, M. Hallek, J. Bernhagen, L. Leng, R. Bucala, A tautomerase-null macrophage migration-inhibitory factor (MIF) gene knock-in mouse model reveals that protein interactions and not enzymatic activity mediate MIF-dependent growth regulation. *Mol. Cell. Biol.* **29**, 1922–1932 (2009). [Medline doi:10.1128/MCB.01907-08](#)
30. A. Kudrin, M. Scott, S. Martin, C. W. Chung, R. Donn, A. McMaster, S. Ellison, D. Ray, K. Ray, M. Binks, Human macrophage migration inhibitory factor: A proven immunomodulatory cytokine? *J. Biol. Chem.* **281**, 29641–29651 (2006). [Medline doi:10.1074/jbc.M601103200](#)
31. E. Rosengren, P. Aman, S. Thelin, C. Hansson, S. Ahlfors, P. Björk, L. Jacobsson, H. Rorsman, The macrophage migration inhibitory factor MIF is a phenylpyruvate tautomerase. *FEBS Lett.* **417**, 85–88 (1997). [Medline doi:10.1016/S0014-5793\(97\)01261-1](#)
32. P. Machanick, T. L. Bailey, MEME-ChIP: Motif analysis of large DNA datasets. *Bioinformatics* **27**, 1696–1697 (2011). [Medline doi:10.1093/bioinformatics/btr189](#)

33. G. Zhao, B. Zhao, Z. Tong, R. Mu, Y. Guan, Effects of 2'-O-methyl nucleotide substitution on EcoRI endonuclease cleavage activities. *PLOS ONE* **8**, e77111 (2013). [Medline](#) [doi:10.1371/journal.pone.0077111](#)
34. A. R. Inácio, K. Ruscher, L. Leng, R. Bucala, T. Deierborg, Macrophage migration inhibitory factor promotes cell death and aggravates neurologic deficits after experimental stroke. *J. Cereb. Blood Flow Metab.* **31**, 1093-1106 (2011). [Medline](#) [doi:10.1038/jcbfm.2010.194](#)
35. M. Bacher, A. Meinhardt, H. Y. Lan, F. S. Dhabhar, W. Mu, C. N. Metz, J. A. Chesney, D. Gems, T. Donnelly, R. C. Atkins, R. Bucala, MIF expression in the rat brain: Implications for neuronal function. *Mol. Med.* **4**, 217-230 (1998). [Medline](#)
36. W. Zhang, L. Li, J. Wang, L. An, X. Hu, J. Xie, R. Yan, S. Chen, S. Zhao, Expression of macrophage migration inhibitory factor in the mouse neocortex and posterior piriform cortices during postnatal development. *Cell. Mol. Neurobiol.* **34**, 1183-1197 (2014). [Medline](#) [doi:10.1007/s10571-014-0094-1](#)
37. T. Calandra, T. Roger, Macrophage migration inhibitory factor: A regulator of innate immunity. *Nat. Rev. Immunol.* **3**, 791-800 (2003). [Medline](#) [doi:10.1038/nri1200](#)
38. J. D. Hudson, M. A. Shoaibi, R. Maestro, A. Carnero, G. J. Hannon, D. H. Beach, A proinflammatory cytokine inhibits p53 tumor suppressor activity. *J. Exp. Med.* **190**, 1375-1382 (1999). [Medline](#) [doi:10.1084/jem.190.10.1375](#)
39. R. Kleemann, A. Hausser, G. Geiger, R. Mischke, A. Burger-Kentischer, O. Flieger, F. J. Johannes, T. Roger, T. Calandra, A. Kapurniotu, M. Grell, D. Finkelmeier, H. Brunner, J. Bernhagen, Intracellular action of the cytokine MIF to modulate AP-1 activity and the cell cycle through Jab1. *Nature* **408**, 211-216 (2000). [Medline](#) [doi:10.1038/35041591](#)
40. S. A. Andрабi, H. C. Kang, J. F. Haince, Y. I. Lee, J. Zhang, Z. Chi, A. B. West, R. C. Koehler, G. G. Poirier, T. M. Dawson, V. L. Dawson, Iduna protects the brain from glutamate excitotoxicity and stroke by interfering with poly(ADP-ribose) polymer-induced cell death. *Nat. Med.* **17**, 692-699 (2011). [Medline](#) [doi:10.1038/nm.2387](#)
41. J. J. Glascock, E. Y. Osman, T. H. Coady, F. F. Rose, M. Shababi, C. L. Lorson, Delivery of therapeutic agents through intracerebroventricular (ICV) and intravenous (IV) injection in mice. *J. Vis. Exp.* **2001**, 2968 (2011). [Medline](#)
42. Y. Chen, N. Negre, Q. Li, J. O. Mieczkowska, M. Slattery, T. Liu, Y. Zhang, T. K. Kim, H. H. He, J. Zieba, Y. Ruan, P. J. Bickel, R. M. Myers, B. J. Wold, K. P. White, J. D. Lieb, X. S. Liu, Systematic evaluation of factors influencing ChIP-seq fidelity. *Nat. Methods* **9**, 609-614 (2012). [Medline](#) [doi:10.1038/nmeth.1985](#)
43. J. Feng, T. Liu, B. Qin, Y. Zhang, X. S. Liu, Identifying ChIP-seq enrichment using MACS. *Nat. Protoc.* **7**, 1728-1740 (2012). [Medline](#) [doi:10.1038/nprot.2012.101](#)
44. H. R. Drew, R. M. Wing, T. Takano, C. Broka, S. Tanaka, K. Itakura, R. E. Dickerson, Structure of a B-DNA dodecamer: Conformation and dynamics. *Proc. Natl. Acad. Sci. U.S.A.* **78**, 2179-2183 (1981). [Medline](#) [doi:10.1073/pnas.78.4.2179](#)

45. T. Masuda, Y. Ito, T. Terada, T. Shibata, T. Mikawa, A non-canonical DNA structure enables homologous recombination in various genetic systems. *J. Biol. Chem.* **284**, 30230–30239 (2009). [Medline](#) [doi:10.1074/jbc.M109.043810](#)
46. A. W. Ghoorah, M. D. Devignes, M. Smail-Tabbone, D. W. Ritchie, Protein docking using case-based reasoning. *Proteins* **81**, 2150–2158 (2013). [Medline](#) [doi:10.1002/prot.24433](#)
47. G. Macindoe, L. Mavridis, V. Venkatraman, M. D. Devignes, D. W. Ritchie, HexServer: An FFT-based protein docking server powered by graphics processors. *Nucleic Acids Res.* **38** (Web Server), W445–W449 (2010). [Medline](#) [doi:10.1093/nar/gkq311](#)
48. P. P. Reddy, V. Raghuram, J. Hradsky, C. Spilker, A. Chakraborty, Y. Sharma, M. Mikhaylova, M. R. Kreutz, Molecular dynamics of the neuronal EF-hand Ca<sup>2+</sup>-sensor Caldendrin. *PLOS ONE* **9**, e103186 (2014). [Medline](#) [doi:10.1371/journal.pone.0103186](#)
49. K. Bendrat, Y. Al-Abed, D. J. Callaway, T. Peng, T. Calandra, C. N. Metz, R. Bucala, Biochemical and mutational investigations of the enzymatic activity of macrophage migration inhibitory factor. *Biochemistry* **36**, 15356–15362 (1997). [Medline](#) [doi:10.1021/bi971153a](#)
50. C. Candé, N. Vahsen, I. Kouranti, E. Schmitt, E. Daugas, C. Spahr, J. Luban, R. T. Kroemer, F. Giordanetto, C. Garrido, J. M. Penninger, G. Kroemer, AIF and cyclophilin A cooperate in apoptosis-associated chromatinolysis. *Oncogene* **23**, 1514–1521 (2004). [Medline](#) [doi:10.1038/sj.onc.1207279](#)
51. C. Artus, H. Boujrad, A. Bouharrou, M. N. Brunelle, S. Hoos, V. J. Yuste, P. Lenormand, J. C. Rousselle, A. Namane, P. England, H. K. Lorenzo, S. A. Susin, AIF promotes chromatinolysis and caspase-independent programmed necrosis by interacting with histone H2AX. *EMBO J.* **29**, 1585–1599 (2010). [Medline](#) [doi:10.1038/emboj.2010.43](#)